NOAA Technical Memorandum ERL WPL-175

REMOTE ATMOSPHERIC PROFILING SYSTEMS FOR TROPOSPHERIC MONITORING

J. C. Kaimal (Editor)

Wave Propagation Laboratory
Boulder, Colorado
January 1990

noaa NATIONAL OCEANIC AND ATMOSPHERIC ADMINISTRATION / Environmental Research Laboratories

NOAA Technical Memorandum ERL WPL-175

REMOTE ATMOSPHERIC PROFILING SYSTEMS FOR TROPOSPHERIC MONITORING

J. C. Kaimal (Editor)

Wave Propagation Laboratory
Boulder, Colorado
January 1990

UNITED STATES
DEPARTMENT OF COMMERCE

Robert A. Mosbacher
Secretary

NATIONAL OCEANIC AND
ATMOSPHERIC ADMINISTRATION

John A. Knauss
Under Secretary for Oceans
and Atmosphere/Administrator

Environmental Research
Laboratories

Joseph O. Fletcher
Director

NOTICE

Mention of a commercial company or product does not constitute an endorsement by NOAA Environmental Research Laboratories. Use for publicity or advertising purposes of information from this publication concerning proprietary products or the tests of such products is not authorized.

For sale by the National Technical Information Service, 5285 Port Royal Road
Springfield, VA 22161

CONTENTS

Acknowledgments

Several scientists in the Wave Propagation Laboratory and the Aeronomy Laboratory contributed with helpful comments, reprints and written text. Among those most helpful were Steven Clifford, Wynn Eberhard, Warner Ecklund, Michael Hardesty, Richard Lataitis, Peter May, William Neff, Judith Schroeder, Richard Strauch, Edgeworth Westwater and Robert Zamora. Their help was invaluable in the preparation of this report. This study was supported by the U.S. Army Atmospheric Science Laboratory under contract ASL 89–8025.

REMOTE ATMOSPHERIC PROFILING SYSTEMS FOR TROPOSPHERIC MONITORING

J. C. Kaimal (Editor)

ABSTRACT. This report addresses a growing need to replace in situ sounding systems currently used in many tropospheric applications with a mobile remote sensing system using a combination of ground and satellite-based technologies. The performance characteristics of both the proven technologies and the new systems are reviewed to determine how they can be combined effectively. An assessment of cost vs. risk is given and several options for combined systems are proposed.

1. INTRODUCTION

Advances in remote sensing during the last 20 years have begun to change the way we observe the environment. Our ability to reach out with acoustic and electromagnetic waves has provided us new insights into the behavior of the atmosphere and the oceans. Advances have also been made in passive remote sensing of temperature and humidity. In many applications such as air quality studies, mesoscale weather forecasting and tactical ground support, remote sensors are slowly replacing in situ sensors.

The Wave Propagation Laboratory (WPL) pioneered many of the remote sensing techniques in use today. Both active and passive systems using electromagnetic (radio and optical) and acoustic signals were conceived, developed, field-tested, and deployed in field experiments by this laboratory during the last 20 years. In this report we draw on our theoretical and field experience to evaluate all potential candidates for a Remote Atmospheric Profiling System (RAPS), with particular consideration to size, mobility and power requirements. On the basis of this study we aim to develop recommendations of systems that should be considered in the design of a prototype for RAPS.

2. BACKGROUND

Vertical profiles of wind speed, wind direction, temperature, and humidity contain important clues to the state of the atmosphere. That information is sought for a broad range of scientific studies and engineering applications. Over the last half century, various techniques emerged to meet this need, each technique to serve a particular application. Balloon-borne rawinsondes became the backbone of upper air observing networks established to provide inputs for weather forecasting, while tower-based sensors provided the low-level information needed for micrometeorological and boundary layer studies. Sensors suspended from tethered balloons proved useful for regional transport and diffusion studies. A host of other techniques, most of them employing immersion sensors transported by one means or the other (e.g., aircraft, rockets, drones, etc) were adopted for various scientific studies. The rapid developments in remote sensing opened up new possibilities; in fact, for many applications remote sensors are increasingly preferred over in situ devices because of the better temporal and spatial coverage. In this section we will discuss the current status of various remote sensing techniques and the promise they hold for tactical deployment.

2.1 AN/GMD Radiosondes

Rawinsonde soundings of the atmosphere are usually obtained using Army/Navy Ground Meteorological Devices (AN GMD–1), Meteorological Data Systems (AN, GN Q3) or Weather Bureau Radio-theodolites (WBRT). These devices automatically track the positions of a weather balloon as it rises through the atmosphere. The radiosonde transmits the pressure, temperature and humidity information to the radio-theodolite. By plotting successive balloon positions as a function of time the winds above the sounding site are estimated.

This sounding technology has been in use since the early 1940's. The reliability of rawinsonde soundings are limited by the representativeness of the observations in space and time, the quality of the sensors used in the instrument packages and the accuracy of the balloon tracking. A rawinsonde sounding usually takes about one hour to ascend to a height of 17 km, and 1.5 hours to the balloon bursting point (ascent rates are usually 300 m/min). When the sounding terminates, the package may be many kilometers from the sounding site. Thus, the data obtained may not represent conditions above the rawinsonde station. Furthermore, temporal changes on scales shorter than two hours are beyond the grasp of the current balloon sounding technology. In high wind situations the radiosonde can be blown so far away from the receiving station that the transmitted signal can no longer be detected. Data losses are significant under these conditions.

The costs of building expendable radiosonde sounding packages limits the accuracy of the temperature, humidity and pressure sensors used in the radiosondes. The National Weather Service determined that pressure errors of ± 1.9 mb are possible in rawinsonde observations. In the same study investigators found that temperature errors of $\pm 0.67°C$ and dew point errors of $\pm 3.4°C$ are also likely in rawinsonde measurements. Since a

relationship between pressure, temperature and humidity is used to determine the height of the package above the surface of the earth these errors introduce an uncertainty into the determination of the balloon position as a function of time. Thus, the accuracy of the winds aloft measurements are compromised by these errors. In addition, the tracking angles measured by the radio-theodolite are only accurate to ±0.05 degrees in azimuth and elevation. Furthermore, at elevation angles smaller than 12 degrees (the limiting angle zone) reflections of the radiosonde transmitted signal off of buildings and nearby structures increases this angular uncertainty. Therefore, the errors in the wind speed measurements may be greater than 10 m/s above 17 km MSL. Wind direction errors are a function of the wind speed. At speeds below 3 m/s +18 degree errors are possible. At wind speeds of 60 m/s this uncertainty decreases to about +2 degrees.

2.2 Wind Profilers

UHF and VHF Doppler radars have been used by investigators for more than a decade to study atmospheric winds. The general acceptance of these instruments by meteorologists has led to a network of thirty 404 MHz wind profilers that will be deployed in the midwestern United States starting in 1989. These instruments give hourly averages of horizontal winds that have a precision of 0.7–1.3 m s^{-1} over a height range from 500 m to 16,250 m AGL. The chosen vertical resolutions of the measured wind components, both horizontal and vertical, are 360 m for the lower- to mid-troposphere and 1000 m for the upper troposphere. Wind profilers have met the original design goal of operating continuously, unattended, and during almost all weather conditions.

The 404 MHz frequency was picked in preference to the 50 MHz and 915 MHz frequencies used in earlier versions of wind profilers. The 50 MHz system (Gage and Balsley, 1978; Ecklund et al., 1979) had the advantage of all-weather operation and greater vertical range (which usually extended well into the stratosphere) but could not provide information in the lowest few kilometers because of recovery problems. It also required too large an antenna (100 m × 100 m). The 915 MHz system (Hogg et al., 1983) tested at Stapleton Airport brought the minimum range down to 300 m at a considerable sacrifice in vertical range (6–8 km). Its triple-beam antenna, consisting of feed horns and large offset parabola is a complex structure but its main disadvantage for meteorological applications is its limited altitude coverage. The 404 MHz system offered a compromise between the two, with its relatively modest antenna size (12 m × 12 m), typical maximum range of 12–15 km, minimum range of 500 m, and vertical resolution of 300 m.

Of particular importance to RAPS are recent attempts in ERL to build transportable versions of the 405 MHz (earlier prototypes used this frequency instead of 404 MHz) and 915 MHz wind profilers. The 405 MHz antenna (Moran et al., 1988) consists of an octagonal array of Yagi elements mounted on a steerable base that can be towed behind the van housing the electronics. The 915 MHz antenna (Ecklund et al., 1988) consists of a truly portable flat microstrip antenna (2.7 m × 2.7 m) operating at low power. Although the two radars have different sensitivities, the two compared extremely well in field tests (Ecklund et al., 1988) to a height of 3 km.

2.3 Radio Acoustic Sounding Systems (RASS)

Recently, an important breakthrough has occurred in temperature sounding through a combination of an acoustic transmitter and a wind profiling radar. First, the speed of the propagating transmitted acoustic energy is measured by the wind profiler. After corrections for vertical air motion and humidity, the temperature can be determined from the propagation speed to a precision of about 0.5°C and with a vertical resolution equal to that of the radar. A temporal resolution of 1–2 min is easily achievable. The upper altitude to which RASS can determine temperature profiles is dependent on the wind and the acoustic attenuation; a research program is underway to determine the limitations. Present estimates suggest that an altitude range of 3.0 km AGL may be routinely achieved with the 405 MHz RASS system. ERL is on the forefront of research in this area.

2.4 Microwave Radiometers

The Wave Propagation Laboratory has routinely operated six–channel microwave radiometers since 1981. Temperature and water vapor profiles are inferred from radiation measurements at six microwave channels and standard surface measurements of pressure, temperature and humidity. Although the device can operate unattended and in almost all weather conditions, the vertical resolution of the profiles is poor, around 100 mb (pressure height thickness) in the lower atmosphere. The strength of this technique is its ability to derive integrated quantities and their time tendencies, of parameters such as geopotential heights and precipitable water vapor, with an accuracy comparable with that of radiosondes and on a time scale of 2 min. Another product of the microwave system is integrated liquid in clouds, a quantity that is of importance to aircraft icing and to climate research. WPL is the leading authority in this area of research.

2.5 High-Resolution Interferometric Sounders (HIS)

The HIS is an infrared instrument that was originally designed by the University of Wisconsin for downward-looking applications from either a satellite or an aircraft; it has recently been operated in an upward-looking mode. The instrument is an interferometer and measures the equivalent of about 1,600 high-spectral-resolution radiation measurements that contain information on temperature and water vapor profiles, as well as some information on ozone and other trace constituents. Temporal resolutions on the order of seconds are attainable. Computer simulations indicate that the accuracies of the derived profiles may be 1.0°C and 15 percent in relative humidity up to about 5 km AGL. The instrument will be adversely affected by partially transparent clouds, but may give good results up to cloud base for opaque clouds. The Ground-based Atmospheric Profiling Experiment (GAPEX) was recently conducted at Denver, Colorado, in which HIS, RASS, and the microwave radiometers were all operated together and compared with two types of radiosonde balloons (Smith et al., 1989). The results of GAPEX may be particularly important in assessing the relative accuracies of the three sounding techniques. NESDIS was instrumental in developing HIS.

2.6 Autocorrelation Radiometers (CORRAD)

The University of Massachusetts has constructed a correlation radiometer that operates in the 20–24 GHz spectral region to derive water vapor profiles. As with the HIS instrument, the limitations of the technique are not clearly defined, and both computer simulations and field testing are required to determine the utility of this technique. WPL has strong connections to this work.

2.7 NOAA Polar-Orbiting Satellites

Thermal soundings from the Tiros-N Operational Vertical Sounder (TOVS) have been routinely available for about a decade. TOVS yields spatially averaged temperature profiles over layers about 200 mb in thickness with rms accuracies of 1°–2°C. The accuracies also depend on cloud conditions and degrade moderately when skies change from clear to partially cloudy to cloudy conditions. The temporal resolution of a single Polar-orbiter is twice-a-day for a given location on the ground, and the nominal horizontal resolution is set at 250 km. Published results have already demonstrated that the temperature retrievals from a ground-based microwave radiometer when combined with retrievals from TOVS are substantially better than those from either system alone. The impact of combining high-vertical-resolution all-weather ground-based soundings with either TOVS or the next generation satellite sounder will be substantial.

2.8 NOAA Geostationary Satellites

The Geostationary Operational Environment Satellite (GOES) provides thermal soundings of temperature and moisture with an instrument called the Visible and Infrared Spin Scan Radiometer (VISSR) Atmospheric Sounder (VAS). The thermal soundings have an effective vertical resolution of about 350 mb and are provided during clear conditions about every hour. The inherent horizontal resolution of the instrument is 7 km, but processing of sounding information reduces the effective resolution to 80 km. The next generation GOES NEXT sounder will have improved vertical resolution and diminished instrumental noise, and may provide a way of improving the horizontal coverage of a network of surface-based sounders. Work already completed with VAS and a limited network of microwave radiometers has shown how such instruments may complement each other.

2.9 Lidars

The WPL Infrared Pulsed Doppler Lidar has emerged as an exciting new tool for plotting wind fields for air quality studies. The new lidar system uses a transverse excited CO_2 laser as its source of coherent radiation. Since the operating wavelength is 9–11 μm in the infrared region, the lidar is most sensitive to the larger atmospheric aerosols, those with radii 1 μm or larger. The lidar is housed in a trailer so that it can be moved to various field experiments. The coherent pulses of infrared radiation are eye-safe at any distance and can be directed throughout the hemisphere above the trailer. Since the aerosols that backscatter radiation to the lidar are moving with the mean wind, this radiation is Doppler-shifted. The Doppler shift is detected by a heterodyne detection technique. For

nominal aerosol loading in the atmosphere (visibility of 40 km), the lidar has a useful horizontal range of 20–30 km. Vertical profiling of winds is accomplished with conical scans using the VAD approach widely employed in radar work. The Doppler lidar has been deployed in field experiments such as studies of drainage winds in a steep canyon in western Colorado, convergence lines and microbursts to the west of Denver's Stapleton Airport, and air pollution episodes in the Boulder–Denver area.

Both Raman and DIAL lidar techniques show promise for measuring atmospheric constituents such as water vapor, ozone, and other trace chemicals. Some of the observations reported are impressive, but sensitivities in some cases are much better at night when background light is low. Work continues in this area. WPL is among the leaders in this field.

2.10 Sodars

The Wave Propagation Laboratory developed several monostatic Doppler sodars (acoustic sounders) capable of measuring winds up to 500 m. Wind speeds and directions are computed from radial wind components detected along two inclined beams and one vertical beam. Acoustic frequencies used in these devices are typically 2 kHz. Several commercial designs exist. The large three-antenna configurations of the past decade are giving way to more compact phased arrays that concentrate more acoustic power in each beam. Minisodars using higher frequencies (~5 kHz) and lighter antennas (nominal range of 10–100 m) have the potential for filling the lowest profiler range gate where information on winds is not available.

3. PROVEN TECHNOLOGIES

In this section we take up some of the more mature remote sensing techniques considered in the previous section and review their performance characteristics in sufficient detail to serve as the basis for evaluating candidate systems for RAPS.

3.1 Wind Profilers

The wind profiler is a ground-based clear-air Doppler radar that can measure vertical profiles of horizontal and vertical wind in nearly all meteorological conditions. There are a number of research radars throughout the world operating in the VHF and UHF bands. Most of the wind profilers that were developed for early applications operated at long wavelengths since height coverage was of prime importance in those applications. Consequently, sensitive receivers with large collecting areas were important, along with high transmitted power. In recent years, the broader capabilities of wind profilers have prompted the use of shorter wavelengths to study atmospheric events in the lower troposphere and even the boundary layer. With lower height coverage requirements the sensitivity of the large systems can be significantly reduced. In this section we will examine the performance characteristics of the wind profilers developed in the Aeronomy Laboratory (AL) and WPL:

a. AL/WPL Platteville VHF profiler (49.82 MHz).

b. WPL Colorado network VHF profiler (49.8 MHz).

c. NOAA 30-station network UHF profiler (404.37 MHz).

d. WPL transportable UHF profiler (404.37 MHz).

e. WPL Stapleton UHF profiler (915 MHz).

f. AL boundary layer profiler (915 MHz).

a. The Platteville VHF Profiler

The radar at Platteville has been described by Ecklund et al. (1979). It has operated continuously and unattended since mid-1981, except for brief periods of downtime caused by computer problems. Since January 1982 data have been tape recorded routinely.

The radar can be operated in a variety of modes because it is computer controlled. It has 3 antenna arrays that are fixed in pointing angle to the zenith, 15° off-zenith to the east and 15° off-zenith to the north. Typical wind profiling operation uses the 3 beam

pointing positions to measure a wind profile every 5 minutes with both low resolution (9-μs pulses) and high resolution (3-μs pulses). Data from each 5 minute cycle of operation are sent to the Profiler computer by dedicated telephone line and the spectral moments are archived. Table 1 summarizes the radar characteristics and typical operating parameters.

Table 1. Platteville radar characteristics and operating parameters.

Radar characteristics	
Frequency	49.82 MHz
Authorized bandwidth	0.4 MHz
Peak power	27 kW (maximum ≈60 kW)
Average power	180 W (maximum ≈1 kW)
Pulse width	3, 9 μs
Antenna aperture	100 m × 100 m, zenith beam 50 m × 50 m, oblique beam
Antenna pointing	zenith, 15° off-zenith to north and east (3 antennas)
Antenna type	fixed phased array of colinear-coaxial dipoles
Two-way beamwidth	2.5° zenith 5° oblique

Operating parameters			
	Vertical mode	Horizontal-wind mode	
	3 μs	9 μs	3 μs
Data processing			
Time domain averaging	2250 pulses	124 pulses	350 pulses
Spectral averaging	2	16	10
Maximum radial velocity	±2.44 m s^{-1}	±19.55 m s^{-1}	±19.55 m s^{-1}
Spectral resolution (64 points)	0.076 m s^{-1}	0.61 m s^{-1}	0.61 m s^{-1}
Tropospheric sampling			
First height	1.85 km	2.5 km	1.7 km
Height spacing	0.45 km	0.9 km	0.3 km
Number of heights	32	18	24

b. The Colorado network VHF profiler

New VHF radars were placed in operation in March, April and May 1983 near Sterling, Craig and Cortez (Strauch et al., 1984). These radars transmit simultaneously in two pointing directions and have 50 m × 50 m antennas. Computers (Data General

Eclipse–120) and data systems perform the complete data analysis at the radar site. Wind profiles are sent by telephone once per hour to the Denver computer. Two resolution modes are used: a 3 μs pulse width for low and middle levels and a 9 μs pulse width to extend the height coverage as high as possible. The data are sampled with 2 and 6 μs gate spacing for the two modes. In the usual sequence of operation, hourly wind profiles are measured using 24 profiles, 12 with each pulse width. The profiles alternate pulse widths and finish the data acquisition cycle in about 45 min. The last 15 min are idle to allow the telephone communication system to poll all the outlying sites and to allow the radar operator to access the station to make changes or obtain diagnostic outputs. The telephone transmission from each site takes about 40 s. Table 2 lists the radar characteristics. Note the unusual pulse repetition periods and number of time domain averages that are selected to reject 60 Hz.

A major current limitation of the VHF radars is the minimum height coverage: about 1.8 km above the surface. During the first few months of testing the lower resolution profiles typically extend to 16–17 km MSL for the hourly averages, but frequently they extend to the highest altitude observed (19 km MSL). At high altitudes the number of profiles in the consensus set decreases because of low SNR. In the high resolution mode the consensus set is often equal to the total number of profiles used (11 or 12) so that individual profiles appear the same as the hourly average. High resolution profiles (with no consensus testing) are available every 95 s. Likewise, the low resolution profiles could be available every 130 s. Data are not currently recorded at the radar site, so these modes are not used because of the telephone time required to transmit the data. Limited archiving at the radar sites will be available for special experiments.

These VHF radars are remotely controlled; every control function that an operator would exercise on site can be performed by telephone. This includes changing parameters such as pulse width, pulse rate, averaging and sampling, and changing the sequencing or operating modes. The major limitation is that the radar has only two electronically controlled bandwidths. In these radars the time domain averaging function is performed by a hardware pre-processor so the minicomputer is not burdened by pulse-to-pulse calculations. Power spectral analysis is performed in software with a Fast Fourier Transform (FFT) algorithm. The time needed to acquire all the radar samples for a single spectrum is about 6 s, so a software FFT is suitable because there are a limited number of range gates. The total data acquisition time for 45 min of total operation per hour is 27.3 min. Less than one-half of the "dead-time" is FFT calculation time. The radar transmitters do not operate during the dead-time or during the last 15 min of the hour. The radar controller/pre-processor and the software are identical for the three sites, and similar hardware and software also operate the UHF radar at Stapleton Airport.

Table 2. Colorado network VHF radar characteristics and operating parameters.

Radar characteristics	
Frequency	49.8 MHz
Authorized bandwidth	0.4 MHz
Peak power	30 kW (maximum ≈60 kW)
Average power	400 W (maximum ≈1 kW)
Pulse width	3, 9 μs
Antenna aperture	50 m × 50 m
Antenna pointing	15° off-zenith to north and east (2 antennas)
Antenna type	fixed phased array of colinear-coaxial dipoles
Two-way beamwidth	5°

Operating parameters		
	Mode 1	Mode 2
Data processing	3 μs pulse	9 μs pulse
Time domain averaging	419 pulses	124 pulses
Spectral averaging	8	16
Maximum radial velocity	± 15.7 m s^{-1}	± 19.6 m s^{-1}
Spectral resolution (64 points)	0.049 m s^{-1}	0.61 m s^{-1}
Height sampling		
First height	1.8 km	3.0 km
Height spacing	290 m	870 m
Number of heights	22	18

c. The 30–station operational UHF profiler

Based on the operating experience with one experimental VHF and UHF system, a number of decisions were made when specifying the profiler to be used in the demonstration network. First, the frequency was selected to be in the 403–406 MHz meteorological aids band because sufficient height coverage can be obtained (not true of 915 MHz) and it appears possible to obtain an operational frequency allocation (not true of 50 MHz). Second, a back-up satellite communication system was specified, in addition to landline, because a significant amount of missing data could be traced to communication problems. The communications is the only subsystem required to have redundancy. Third, the reliability of the wind profiler was required to be six months mean-time-between-failure (MTBF); this is higher than for most radars, but experience with the experimental network showed it was achievable. Fourth, because of experience with normal sidelobe antennas at 400 MHz, a low sidelobe antenna was specified. It is important, when operating near thunderstorms, to reject hydrometeor returns in the antenna sidelobes region. Fifth,

the experimental network showed that at least three different antenna technologies could be used for wind profiling, but it was not clear which was the most cost-effective approach.

The significant operational and maintenance features of the wind profiler system design now in progress are:

1. Unattended Operation
   - Minimum MTBF of 6 months.
   - Remote maintenance monitoring and control.
   - Satellite and land automated digital communications.
2. State-of-the-Art Technology
   - High efficiency solid-state transmitter.
   - Low sidelobe antenna.
   - Digital signal/data processing.
   - Microprocessor performance monitor.
3. High Accuracy
   - Wind speed corrected for vertical velocity.
   - Wind speed within 1 m s^{-1}.
   - Frequent measurements (10 per hour).
4. Convenient Installation
   - Approximately 3000 square feet total installed area.
   - Transportable shelter houses all electronics equipment in controlled environment.
   - Prefabricated steel antenna support sections.

Using a dual planar array of coaxial collinear antenna elements, the wind profiler generates three sequential beam positions, one vertical and two oblique patterns, under computer control to detect Doppler frequency shifts in the return signal reflected from temperature and humidity fluctuations. These frequency shifts, in combination with beam position, are translated into accurate wind speed and direction data (see Table 3). It should be pointed out that the 350 m height resolution listed is strictly a function of the bandwidth allocation for the network (restricted to limit interference with other users). With broader bandwidth, the 404 MHz system can potentially measure winds with a 100 m vertical resolution.

Table 3. Characteristics of the 30 station operational UHF Profiler.

Frequency	404.37 MHz	
Bandwidth	0.5 MHz	
Peak power	16 kW	
Average power	2 kW	
Antenna aperture	12 m × 12 m array of 400 Co-Co antennas	
Beamwidth (3 dB one way)	4°	
Gain	32 dB	
Antenna pointing	73.3° elevation nominally north and east	
Operating modes	1.67 μs pulse	6.67 μs pulse
Pulse repetition period	100 μs	153 μs
Average power	1 kW	2 kW
Time domain averages	119	52
Spectral averages	39	58
Maximum radial velocity	± 16 m s^{-1}	± 24 m s^{-1}
Spectral resolution	0.125 m s^{-1}	0.188
Data collection period 3 beams, 10 profiles	60 min	60 min
Height resolution (73.3° elev.)	350 m	1 km
Farthest gate (73.3° elev.)	9.25 km AGL	17.25 km AGL

The wind profiler has two modes of operation, a high mode to measure winds to a maximum height and a low mode to measure winds to moderate heights but with improved height resolution. Normal operation consists of alternating between these two modes during a basic two-minute measurement period and transmitting the processed data back to the display/processing Hub at the end of a 6 min period with summary data each hour. During each period, the profiler sequentially switches the antenna beams 16.7 deg from the vertical to the east, to the north, and then to the vertical. In high mode, range gates provide for coverage from a height of 7.5 km to 16.25 km. In low mode, range gates provide for coverage from a height of 0.5 km AGL to 9.25 km. These range gates consist of 36 equally spaced time samples (which are a function of beam angle) between the specified minimum and maximum heights.

The system operates on a nominal 6 min cycle and also on an hourly summary cycle both keyed to the hour. During each nominal 6 min period, data are collected, processed, stored, and then transmitted by landline to the Hub prior to the completion of the next 6 min period. After each hourly cycle, key data from each 6 min period are consensus-averaged and, at a site-specific offset time after each hour, transmitted via GOES satellite to the Hub.

Meeting the most stringent of environmental conditions, the equipment shelter houses and maintains the wind profiler electronics at constant temperature and humidity. Designed from initial concept for unmanned operation, the system continuously monitors all

pertinent performance parameters to ensure an extremely high confidence level in output wind data accuracy.

d. The transportable UHF profiler

The transportable 404.37 MHz lower tropospheric radar built by WPL (Moran et al., 1989) has a power aperture product of about 800 Wm^2 and has routinely seen to heights of 5–6 km during both the dryer winter and moister summer months.

The radar's characteristics are given in Table 4. The radar's antenna is a mechanically scanned array of 76 Yagi elements mounted on a lightweight wood and fiberglass platform. The azimuth rotation of 400° and elevation tilt of 25° allow beam positioning similar to that used in other profilers. The radar electronics are mounted in a van, and the antenna is mounted on a small trailer and can be folded for transport.

The array of Yagi elements is power tapered to reduce side lobes, and a ground screen is fitted under the array to reduce interaction with the near field environment,

Table 4. Characteristics of transportable UHF wind profiler.

Frequency	404.37 MHz	
Bandwidth	1 MHz	
Peak power	1.2 kW	
Average power	100 W (max)	
Antenna aperture	5.5 m diameter array of 76 5-element Yagis	
Beamwidth (3 dB one way)	7.6°	
Gain	25.3 dB	
Antenna pointing	65° to 90° elevation 0° to 360° azimuth	
Operating modes (typical)	1 μs pulse	3 μs pulse
Pulse repetition period	40 μs	80 μs
Average power	30 W	45 W
Time domain averages	280	124
Spectral averages	12	16
Maximum radial velocity	$\pm$16.5 m s^{-1}	$\pm$18.7 m s^{-1}
Spectral resolution	0.52 m s^{-1}	0.58 m s^{-1}
Data collection period 4 beams, 12 profiles	22 min	26 min
Height resolution (75° elev.)	145 m	290 m
Farthest gate (75° elev.)	4.73 km AGL	7.43 km AGL

including the trailer. A small electronically opaque fence (5 cm wire) is anchored to the edge of the platform and rotates with the antenna. The fence is tilted 45° to the plane of the platform and is effective in reducing low-angle sidelobes by more than 10 dB. Recent tests with the antenna in moderate clutter environments (near the foothills of a mountain-

ous region) emphasize the need for a higher quality antenna for many observational applications. An antenna that is not elevated as this one is, and does not tilt its sidelobes toward the nearby clutter, would generally improve the clutter performance.

The electronics and processing used in the radar are identical to those used in other WPL profiling radars (Strauch et al., 1984). The power amplifier (1200–W peak, 10% duty cycle max) is similar to the modules used in the NOAA network radars. A special pulse-to-pulse phase-coding scheme is needed in this type of radar to reduce the sensitivity of detection of the radar's transmitter by SARSAT receivers.

The vertical profile of horizontal winds is calculated from radial velocity estimates along four orthogonal beam-pointing directions (N,E,S,W). No direct measurement of vertical velocities is made; however, vertical velocities can be inferred from radial estimates of two co-planar beams. The effects of vertical velocity are removed by using co-linear beam data, and 12 estimates are compared over a half-hour interval to determine a subset that meets a consensus requirement. Those velocities for each direction that meet the consensus are averaged and form the vector components of wind for each range. This technique has been shown to have an overall accuracy of 0.7–1.3 m s^{-1} when corrections were made for vertical velocities (Strauch et al., 1987).

e. The Stapleton UHF profiler

The 33 cm (915 MHz) radar (Hogg et al., 1983) has been in operation since February 1983. It uses a single transmitter and an offset paraboloidal antenna with three offset feeds to produce the zenith and oblique pointing directions sequentially. Table 5 lists characteristics and typical operating parameters. This radar has three electronically selectable bandwidths; 1, 3 and 9 μs pulses are transmitted. As in the Colorado network VHF radars, range gate spacing is two-thirds of the pulse width. Data processing hardware and software are essentially the same as those described for the VHF systems; printout formats and operator control are identical. This radar detects clouds and precipitation, so correction for hydrometeor fallspeeds is needed.

One limitation of this system is that the data processing time exceeds the data acquisition time. The wavelength and (therefore) the time needed to acquire the data for a single spectrum are one-eighteenth those of the VHF radars. The software FFT calculation time for the 33 cm radar exceeds the dwell time, thereby reducing the effective observation time. The use of array processors could alleviate this problem and a new generation of computers will be replacing the old Data General S–120 minicomputer.

Table 5. Stapleton Profiler characteristics and operating parameters.

Radar characteristics

Frequency	915 MHz
Maximum bandwidth	2 MHz
Peak power	5.6 kW
Duty cycle	<25%
Pulse width	1, 3, 9 μs
Antenna aperture	≈10 m × 10 m
Antenna pointing	zenith 15° off-zenith to north and east
Antenna type	offset paraboloidal reflector with offset horn feeds
Two-way beamwidth	1.7°
System noise temperature	240 K

Operating parameters

	Mode 1	Mode 2	Mode 3
Data processing			
Pulse width	1 μs	3 μs	9 μs
Pulse repetition period	50 μs	64 μs	110 μs
Average power	110 W	260 W	450 W
Time domain averaging	136 pulses	80 pulses	46 pulses
Spectral averaging	8 spectra	32 spectra	32 spectra
Maximum radial velocity	±12.02 m s^{-1}	±15.97 m s^{-1}	±16.16 m s^{-1}
Spectral resolution (64 points)	0.376 m s^{-1}	0.499 m s^{-1}	0.505 m s^{-1}
Height sampling			
First height	0.35 km	1.64 km	2.7 km
Height spacing	100 m	290 m	870 m
Number of heights	24	24	18

A more fundamental limitation relating to radar wavelength may be the radar's inability to obtain wind measurements routinely at altitudes above 10 km; turbulent scales measured by clear-air radars may not be in the inertial subrange of turbulence in the upper troposphere. If the $\lambda/2$ scale sizes are in the inertial subrange then the clear-air radar reflectivity is given by $0.38\ C_n^2\lambda^{-1/3}$ where C_n^2 is the refractive index structure constant and λ is the radar wavelength. However if $\lambda/2$ turbulent scales are damped by viscosity then radar reflectivity decreases abruptly. Figure 1 shows how the cutoff of radar reflectivity varies with altitude for various levels of mechanical turbulence. For years it

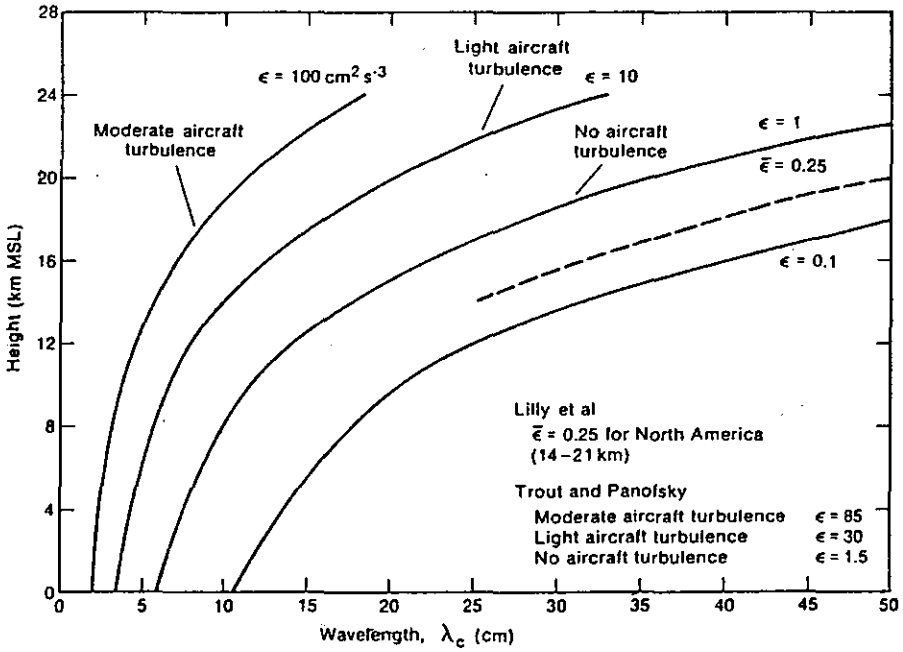

Figure 1. Cutoff wavelength (λ_c) vs. height for various levels of mechanical turbulence (ϵ). Routine clear-air wind profiling should be possible with radar wavelengths greater than λ_c, i.e., to the right of the curves.

has been noted that high-power 10 cm radars measure a sharp decrease in clear-air radar reflectivity above the convective boundary layer. These radars observe elevated layers on occasion. Figure 1 suggests the reason that 10 cm wavelength Doppler radars can measure low-level winds but are not suitable for routine clear-air wind profiling above about 5 km MSL. It appears that a radar with 33 cm wavelength will also be limited in height coverage. Our early results show that wind profiles can usually be measured to 10 km MSL with the 33 cm radar. Note from Table 5 that this radar has less sensitivity than many 10 cm Doppler radars that cannot measure wind profiles above the boundary layer. However, coverage above 10 km with the 33 cm radar depends on the particular conditions.

f. Boundary layer UHF profiler

A prototype UHF boundary layer wind profiler is under development at the Aeronomy Laboratory (Ecklund et al., 1987). This device is being developed to operate in a "hybrid" mode with our large 50 MHz profilers in the tropical Pacific to fill in the lower few km not covered by the large radars. The boundary layer profiler can also be employed as a stand-alone device to study a number of important boundary layer problems. In the following sections we outline the general features of the BLR and describe initial results obtained in Colorado and at our site on Christmas Island in the central equatorial Pacific.

The need for fast system recovery (minimum height coverage to about 100 meters above the surface) and the need for a small antenna dictated operating at 915 MHz. The main disadvantage of this relatively high frequency for wind profiling is the enhanced

sensitivity to hydrometeors. Under precipitation or in heavy clouds the radar signal will be dominated by scattering from hydrometeors and the determination of vertical air motion will not be possible. However, to the extent that hydrometeors are advected by the mean winds, it is possible to obtain a profile of the horizontal wind in rain.

A microstrip panel antenna was developed for use with this profiler since it satisfied requirements for a rugged, transportable antenna that could be mounted low to the ground (to suppress ground clutter). A prototype 0.9 by 1.8 m antenna was mounted on a rotator, and the 915 MHz (100 Watt peak power) transmitter was mounted under the antenna. The antenna was installed inside a fence to reduce clutter from buildings, power lines and mountains. The initial radar controller and signal processor were adapted from existing 50 MHz profilers. This system could sample 30 heights at a time with 150 meter resolution, coherently integrate the samples, and compute and average the FFT's. The resulting averaged spectra are tape recorded and were also available for video display.

A prototype unit was operated intermittently from 11 August to 1 November 1986. Sample wind profiles were obtained in Colorado under a variety of conditions ranging from clear skies to heavy thundershowers. In general, the boundary layer profiler was able to observe up to about 1500 meters in clear air with 150 meter height resolution and with an average power aperture product of 2 Wm^2. On some occasions, however, the height coverage was higher or lower than this in agreement with other clear-air radar studies which have shown that the extreme range of radar reflectivity covers more than two orders of magnitude. As expected, the maximum observable height range increased dramatically under precipitation conditions.

In November 1986, a preliminary test of the profiler was carried out near the Equator, south of Hawaii, at Christmas Island (Ecklund et al., 1989). The antenna was 0.9 by 0.9 m, the transmitted power was 1 Watt (average), height resolution was 150 m and the observing time per record was 1 minute. The profiler in this configuration observed essentially continuous echoes to 1800 meters. More recently (May-June 1988) observations made at Flatville, IL demonstrated how well the boundary layer profiler can detect near-surface features like low-level jets. Figure 2 shows an example of a low-level jet in the meridional wind component observed during the nighttime hours. The surface wind speed was less than 1 m s^{-1}, but the radar showed a southward wind component of nearly 10 m s^{-1} at a height of 500 m above the ground.

A new PC-based controller/signal processor has been developed by the Aeronomy Laboratory in 1989. The new system can operate with a range resolution of 30 m, substantially more powerful and less expensive than earlier systems. Table 6 lists the characteristics and operating parameters of the new system.

Table 6. Boundary layer Profiler characteristics and operating parameters.

Radar characteristics	
Frequency	915 MHz
Bandwidth	5 MHz
Peak power	300–600 W
Average power	5–15 W
Pulse width	0.2–2.7 μs
Antenna aperture	formed by 0.9 m × 0.9 m antenna modules (typically 2–9 m^2)
Antenna pointing	fixed beams (3) or mechanically steered (rotated in azimuth at fixed elevation)
Antenna type	microstrip panel array
Typical operating parameters	
Pulse repetition period	30–100 μs
Number of spectral points	64
Maximum radial velocity	±10 m/s
Height range (sampled)	100 m – 4.5 km
Sample spacing	30–400 m
Number of samples	30–50
Real-time processing efficiency	80–100%

3.2 Radio Acoustic Sounding Systems

RASS is a promising method for remotely sensing temperature profiles by combining radar and acoustic techniques. The radar detects backscattered radiation from fluctuations in the refractive index of the air induced by a sound wave. The Doppler shift of the backscattered signal gives an estimate of the speed of sound and therefore virtual temperature. Clear-air wind-profiling radars can be easily adapted to the RASS technique (Strauch et al., 1988; Currier et al., 1988) and the height coverage for the temperature profiles obtained with these radars is significantly greater than with earlier RASS systems that used radars with less sensitivity and simple data-processing procedures. Here we examine the height coverage of RASS measurements at three frequencies and factors limiting the performance of the systems. Strong backscatter of the radar signal is obtained when (1) the wavelength of the acoustic signal is matched to half of the radar wavelength, i.e., the Bragg condition is satisfied, and (2) the effect of the (almost) spherical acoustic wavefronts results in the backscattered signal being focused onto the antenna. For our tests, the Bragg condition was assured by transmitting a range of acoustic frequencies in a frequency modulated continuous wave (FM-CW) sweep.

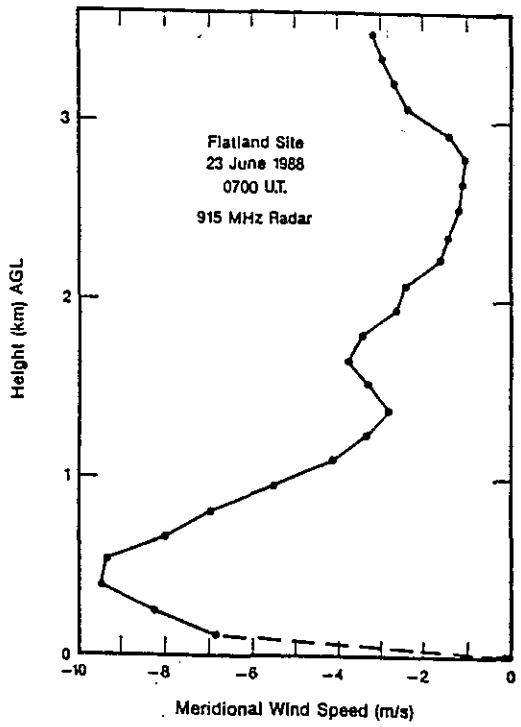

Figure 2. Low-level jet observed by the boundary layer profiler.

We used three wind profilers operating at frequencies of 49.8, 404.37 and 915 MHz. Acoustic frequencies of about 110, 900, and 2000 Hz respectively were Bragg matched to these radars. The characteristics of each of the systems is given in Table 7. Each of the radars is a monostatic, pulsed Doppler radar capable of receiving signals from the clear-air with a vertically pointed radar beam. The radars operate in the same manner as for the clear air wind measurements, except that the receiver's local oscillator is offset in frequency to allow the detection of Doppler shifts corresponding to sound velocities of around 330 m s^{-1}. Sophisticated signal processing allows the accurate measurement of the Doppler shift of the RASS echo at signal-to-noise ratios (SNR) as low as -35 dB (May and Strauch, 1989). This is a major factor in the extended height coverage reported here compared with many earlier RASS systems. The random sample consensus algorithm is also applied to a series of profiles to eliminate signals which are far from the norm (Strauch et al., 1984). There are three effects limiting the range coverage. The first is geometric, in that the wind displaces the spot away from the radar, so that at some height there is no longer a detectable signal from the sidelobes or wings of the spot. The displacements also result in path differences from the radar to different parts of a given acoustic wave front, thus reducing the coherence of the backscattered signals. Second, turbulence acts to smear the spot by decreasing the transverse coherence of the acoustic wavefronts of the acoustic signal (Clifford et al., 1978). Theoretical studies (Clifford et al., 1978; Kon, 1984) have suggested that for strong turbulence the signal power should decrease as $r^{-26/5}$ instead of the r^{-2} dependence obtained because of the spreading of the acoustic wavefront (no turbulence),where r is the range. The final effect is that of acoustic attenuation which is a strong function of frequency, being almost negligible at 110 Hz,

Table 7. Characteristics of RASS/wind profiler systems operating at three radar frequencies.

Site	Platteville	Erie	Denver
Characteristic			
Radar			
Frequency (MHz)	49.8	404.37	915
Wavelength (m)	6.0	0.7414	0.3
Antenna size (m^2)	10,000	25	100
Beamwidth (1 way) (degrees)	3	7.8	2
Range resolution (m)	300	150	150
Mean power (W)	200	30	100
Sampling time (1 profile) (min)	1	1	1
Acoustic			
Frequency (Hz)	~110	~900	~2000
Beamwidth (1 way)	~60°	~17°	~8°
Acoustic power (W)	50	5	50
RASS Altitude Coverage			
Min. altitude (km)	2.1	0.4	0.2
Max. altitude (km)	5–9	1.5–2.5	0.7–1.5
Observation period (1988)	May-Jun	Jan-Feb	Mar-Apr

but reaching around 40 dB km^{-1} at 2000 Hz for some values of temperature and humidity (Harris, 1966).

Examples of typical temperature and power profiles obtained with the radars at three different frequencies are shown in Fig. 3; the solid line shows the temperature profile obtained by radiosondes launched within a few hundred meters of the radar. Agreement between the two temperature estimates is generally excellent, with mean differences of a few tenths of a degree. In the case of the 50 MHz profile, there is a region between 3 and 5 km where the RASS measures a greater temperature than the sonde. This is associated with a region of greater than 90% relative humidity, so that there is a significant difference between the temperature and virtual temperature measured by the RASS. The individual RASS measurements are also shown; most of the fluctuations are attributed to vertical air motions that were not observed directly in this study. However, in normal operation a wind profiler can measure vertical wind speed. We note that these fluctuations may be large since the radars are all located in the lee of the Rockies.

Temperature profiles up to about 5–9 km are typically seen with the 49.8 MHz RASS/wind profiler. The study of Masuda (1988) used a raytracing algorithm to calculate the position of the acoustic phase fronts in order to calculate the position of the spot. A

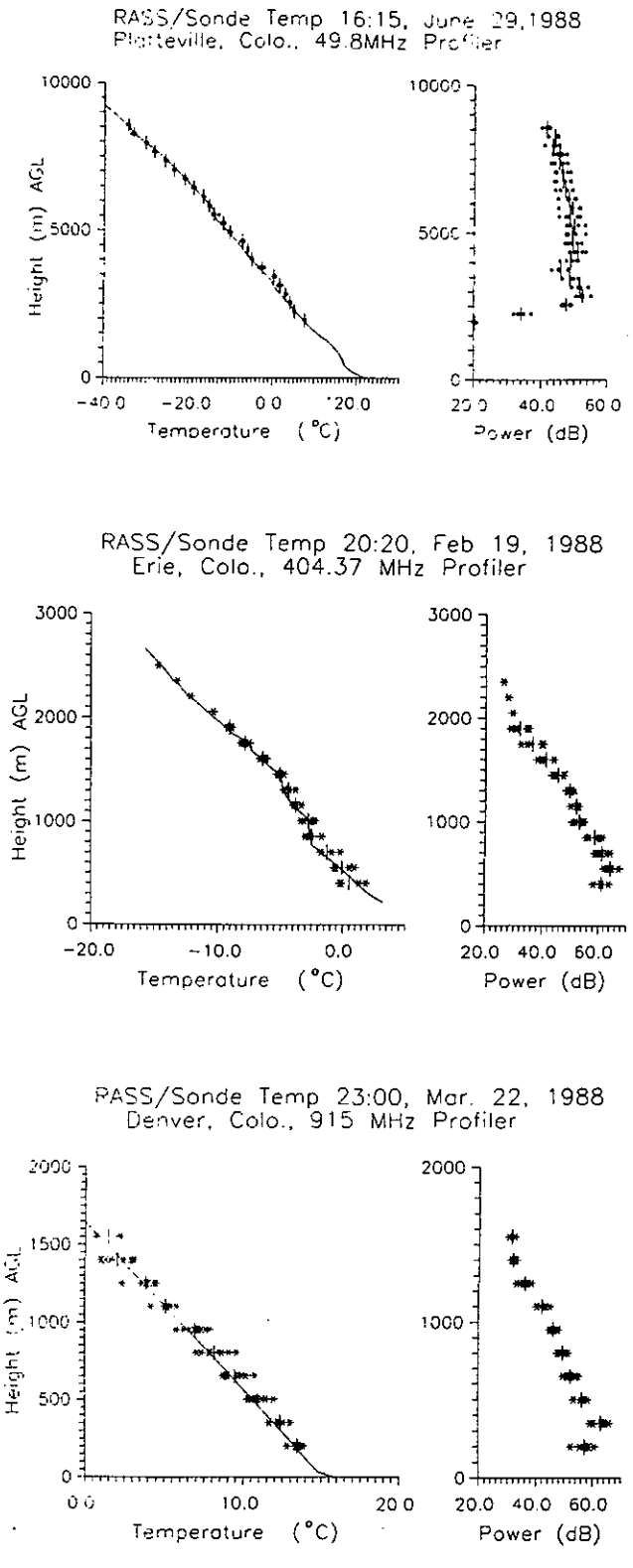

Figure 3. Profiles of power and temperature for the three RASS/wind Profiler systems operating at (a) 49.8, (b) 404.37 and (c) 915 MHz. Individual RASS observations are marked by the stars and the mean values by the small vertical bars. The solid line is the temperature profile measured by a radiosonde launched next to the radar.

similar approach for a radar with a vertically pointing antenna of 100 m diameter indicates that the spot will be focused onto some part of the antenna for measurements up to about 6 km for the wind conditions encountered during this study, which is in reasonable agreement with the observed range. The effect of turbulence on the acoustic wavefronts (frequency ~110 Hz) is not as important for this longer wavelength. It is sometimes seen that the backscattered power has an approximate r^2 range dependence, further indicating that turbulence is not important for this wavelength.

The 404.37 MHz radar typically obtained measurements up to about 2.5 km above ground. Acoustic attenuation provided one important limitation at this intermediate frequency with theoretical values of about 10 dB km^{-1} indicating that other effects such as turbulence may play a role. Observations were made under strong wind conditions, but the range covered was not strongly affected. A raytracing calculation showed that the focused condition will be obtained only below 1 km under most conditions. Since we see to altitudes more than a factor of 2 greater, it suggests that turbulent distortion of the acoustic wavefronts acts to defocus the spot and give significant signal levels to the radar. Thus it appears that turbulence has two effects: (1) to decrease the acoustic wavefronts lateral coherence and thus to decrease the intensity of the spot signal, and (2) to smear the backscattered radiation over a larger area (Clifford et al., 1978) and thus allow the detection of the acoustic signal over a wide range of conditions using a sensitive radar. Although the RASS/wind profiler systems have different sensitivities, the rapid decrease in backscattered power with increasing altitude makes qualitative comparisons between the systems valid. For example, the 915 MHz radar is much more sensitive than the 404.37 MHz radar, but it has worse performance for RASS because of its operating frequency.

Contrasting the low frequency observations with those performed with the 915 MHz radar shows that the latter are sharply limited by such effects as turbulence and acoustic attenuation. In particular the performance of the 915 MHz system was strongly correlated with the humidity; being better at high relative humidity, since the acoustic attenuation at temperatures around 0°C decreases sharply with increasing humidity (Harris, 1966). Turbulent distortion of the acoustic wavefronts in the boundary layer is probably important at this short wavelength.

Independent tests conducted with the Aeronomy Laboratory's boundary layer profiler in conjunction with a simple acoustic source showed good agreement with rawinsonde temperature measurements up to a height of about 1 km. The acoustic source used in the test was a commercial 75 Watt driver connected to a horn with a 0.9 by 0.9 m aperture. The pulsed Doppler radar operated at 915 MHz with a peak power of 300 Watts and used a vertically-directed 1.8 by 1.8 m panel antenna. The radar height resolution was either 75 or 150 meters during the tests. The acoustic source was linearly swept from 2030 to 2080 Hz during a one minute interval. At the same time the radar was operated in a mode that obtained averaged Doppler spectra with good frequency resolution so that the acoustic frequency corresponding to the peak of the averaged Doppler spectra could be determined

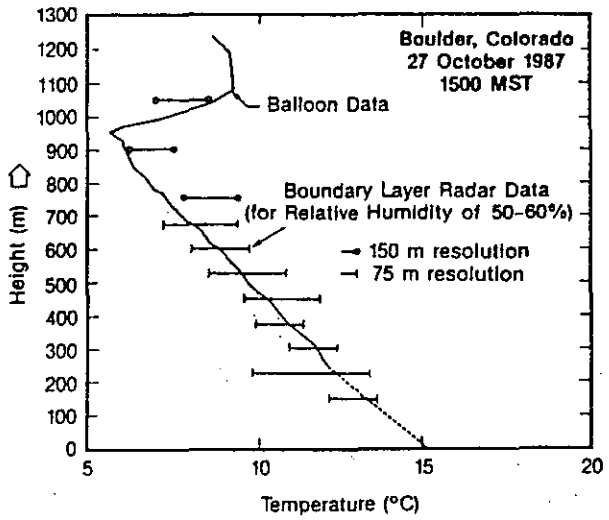

Figure 4. Boundary layer profiler RASS temperature profile vs. balloon measured profile.

at each height. The averaged spectra were recorded and plotted for later analysis. During the radar-acoustic sounding period a balloon sonde was launched about 50 meters from the radar. The sonde measured both dry and wet-bulb temperatures at 30 meter height intervals.

A temperature profile taken during the test is shown in Fig. 4. The horizontal bars show the range of four radar-acoustic determinations of temperature made over a 20 minute time interval centered on the balloon sounding time. The radar height resolution is 75 meters from 150 meters to 675 meters above the surface and 150 meters for the values shown at heights of 750, 900 and 1050 meters. The radar-acoustic values have been corrected for the sound speed at a relative humidity of 50 to 60% (measured by the balloon sonde). No correction has been made for vertical wind velocity in this comparison.

3.3 Microwave Profilers (MWP)

Since 1981, WPL has operated a six-channel microwave radiometer at Stapleton Airport in Denver, Colordo. The principal products of the MicroWave Profiler (MWP) are low-resolution vertical temperature profiles and integrated amounts of water vapor and cloud liquid water. The radiometer measures brightness temperatures at six frequencies. Table 8 shows the center frequencies for each of the six channels used in the MWP.

Choice of microwave frequencies appropriate for remotely sensing the temperature and humidity is governed by the wavelengths of oxygen and water vapor absorption lines. Oxygen absorbs over a band of frequencies from roughly 50 to 70 GHz, and also at 118 GHz, whereas water vapor has absorption lines near 22 and 183 GHz. Absorption by liquid water, on the other hand, increases monotonically with frequency over the entire

Table 8. Center frequencies for channels used in the MWP system.

Channel	Frequency	Atmospheric constituent most effective	Bandwidth (GHz)
1	20.60	water vapor	1.0
2	31.65	liquid	1.0
3	52.85	temperature	0.1
4	53.85	temperature	0.1
5	55.45	temperature	0.1
6	58.80	temperature	0.1

microwave band. Since a large amount of liquid (i.e., rain), limits the capability of radiometers, it is preferable, for all-weather operation, to utilize the lowest microwave frequencies possible. In the prototype MWP, a frequency near 22 GHz is used primarily for vapor, and the 50–60 GHz band for temperature. Oxygen, with its constant mixing ratio, is an ideal gas for radiometric measurement of temperature. A frequency near 30 GHz, well removed from the oxygen and vapor absorption lines, is used primarily for measurement of zenith-integrated liquid. Ice particles and dry snow have negligible absorption, and therefore produce no effect on the microwave radiometers. Table 9 lists the channel characteristics and operating parameters of the MWP.

The frequency primarily for vapor measurement is 20.6 GHz rather than 22.235 GHz, which is the frequency of the peak of the absorption line. This off-line-center choice is made because the derived total amount of vapor is then relatively independent of the pressure (i.e., height) of the vapor.

The four channels 52.85 through 58.80 GHz are located on the low-frequency side of the oxygen absorption band. The lowest absorption of these therefore occurs at 52.85 GHz, and emission from the entire troposphere is sensed effectively by this channel. On the other hand, 58.80 GHz is a highly absorbing channel, and significant emission is received from only the lowest kilometer of the troposphere. The 53.85 and 55.45 GHz channels, which absorb at strengths intermediate between the other two, are sensitive mainly to the oxygen up to mid-altitudes (e.g., 2 to 6 km above the surface). By combining of the emission in all of these channels, profiling is achieved.

All six radiometer channels are of similar design, but the bandwidths of the channels differ, as indicated in Table 8. The channels used for temperature sensing utilize a relatively narrow bandwidth (0.1 GHz) to provide sufficient discrimination between channels.

The antenna beams for all channels point to zenith, and have essentially the same shape and beamwidth. The latter is an important feature in properly accounting for liquid-bearing clouds that pass through the beams. If the beamwidths were unequal, a liquid-bearing cloud entering the system would produce a "signal" in some channels, and none in the others, and correction of the retrieved temperature and humidity for the emission

Table 9. MWP characteristics and operating parameters

Channel characteristics

Channel number	Frequency (GHz)	Wavelength (cm)	Effective antenna area (cm^2)	3 dB beam-width (degrees)	Averaging time (min)	Brightness Temperature accuracy	Brightness Temperature sensitivity
1	20.60	1.455	1416	2.5	2.0	1.05	0.047
2	31.65	0.947	600	2.5	2.0	0.75	0.046
3	52.80	0.567	215	2.5	2.0	0.86	0.200
4	53.85	0.577	207	2.5	2.0	0.63	0.187
5	55.45	0.541	196	2.5	2.0	0.90	0.077
6	58.80	0.510	174	2.5	2.0	0.64	0.094

Vertical resolution

Temperature profile	~1/2 height above ground
Humidity profile	~ 1 scale height ≈ 2.5 km

by the liquid in the cloud would not be feasible. The antennas for all channels are offset paraboloids located inside the Profiler building. Emission from the zenith is reflected by the 45° flat reflector, through a microwave window protected by a cowling, to the paraboloids where it is focused into the radiometers. Each of the three paraboloids accommodates two channels. The 45° flat reflector is scannable in elevation angle for calibration purposes.

The electronics and parabolic antennas are housed in a trailer whose temperature is controlled to within ±5°C; over a year's time, the internal temperatures of the instrument vary by less than ±1°C. Internal calibration of the instrument is achieved by sequentially switching between the antenna and two reference black bodies. External calibration procedures require "tipping curves" and/or radiative transfer calculations based on radiosondes. Calibration factors require infrequent updating, perhaps once a month.

Temperature, water vapor, and cloud liquid are derived every two minutes from the radiometer, using a profile retrieval technique known as linear statistical inversion (Westwater and Strand, 1968). The statistical accuracies of the derived parameters have been evaluated by comparison with National Weather Service radiosondes (Westwater et al., 1985). The rms accuracies of derived precipitable water vapor and geopotential heights to 500 mb are comparable to those of radiosondes. Above the first kilometer AGL,, the vertical resolution of temperature profiles degrades rapidly, with the consequence that elevated inversions are not resolved.

It has been recognized for some years that knowledge of heights of significant and persistent changes in temperature (or humidity) can be used to improve retrieval of radiometric profiles. It has been shown (Miller and Falls, 1989) that a simple extension of linear statistical inversion (Westwater and Strand, 1968) can naturally assimilate significant height information into the retrieval process. Essentially, this extension restricts *a priori* profiles that are used to construct retrieval coefficients to a subset containing pro-

files that possess only the desired significant height within a given altitude band. Linear retrieval coefficients then are derived from the restricted subset in the usual way. Consider, for example, a radar-indicated height of the base of an elevated inversion at 2 km, and a resolving power of the radar of ±200 m. Then, to couple the radar information with that of the radiometer we would use radiometric retrieval coefficients derived from an *a priori* ensemble of profiles that contained base heights of elevated inversions from 1.8 to 2.2 km. In practice, the resolution window's width must be consistent with the resolution of the radar, and the window should be large enough to include a sufficient number of *a priori* profiles to allow construction of the retrieval coefficients with statistical confidence.

This technique has been applied to numerous computer-simulated retrievals; a typical one is shown in Fig. 5. Here both radiometer and radiosonde data are measured (Decker et al., 1978), but the inferred radar height was simulated by assuming that the height of the base of the elevated (tradewind) inversion was known to within 20 mb (~200 m). Note the dramatic improvement in accuracy in the retrieved temperature and humidity profiles when the height information is included.

In addition to this computer simulation, field experiments (Decker, 1978) have been conducted using both active and passive sounders. These experiments provide an example of the use of clear air returns obtained by a 10 cm wavelength radar (Chadwick et al., 1976) in improving temperature profile retrieval (see Fig. 5). These data were obtained at the Boulder Atmospheric Observatory (BAO) near Boulder, Colorado, 6 September 1978.

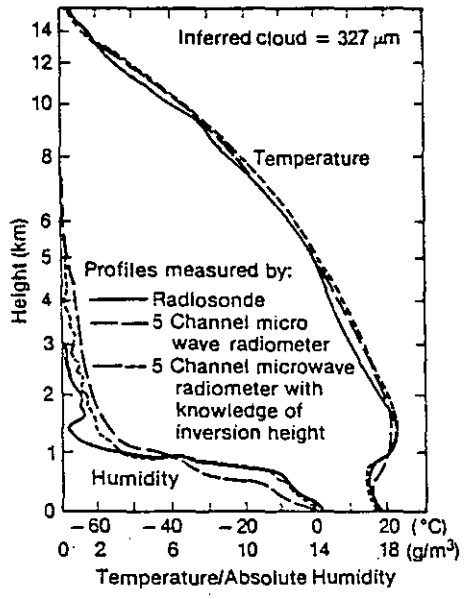

Figure 5. Computer-simulated radiometric temperature and water vapor profile retrievals with and without information on the height of the inversion at about 1 km.

The radiosonde profile is from a conventional system operated by the National Center for Atmospheric Research (NCAR). The radiometric data were measured with a ground-based version of the SCAMS radiometer which was operated by personnel from the Jet Propulsion Laboratory. These measurements include zenith radiation at five frequencies plus 55.45 GHz measurements at a zenith angle of 59.3 degrees. (This sixth observation was taken to simulate use of the 58.8 GHz zenith channel used in the MWP system.) By

using these six measurements and measurements of surface temperature, pressure and relative humidity, the profile designated "Radiometer, No Height Information" of Fig. 6 was obtained. As expected, this profile smooths the elevated temperature inversion evident in the radiosonde profile. At the time of the radiometric measurement, a persistent echo was observed at 190 m above the surface by a 10 cm wavelength radar. We now include this information in the temperature profile retrieval process by assuming that the radar echo represents the base of an elevated temperature inversion. Statistical coefficients were derived from the set of *a priori* profiles that contain elevated temperature inversion bases between 10 and 30 mb pressure difference from the surface. The resulting profile, designated "Radiometer with Height Information" of Fig. 6, now exhibits the structure of the radiosonde profile.

In addition to measuring low altitude features of temperature, VHF radars are also capable of measuring tropopause height (Gage and Green, 1979). The tropopause height information can be inserted into a temperature retrieval algorithm using the restricted-ensemble technique discussed above. The data shown in Fig. 7 were used in the retrieval algorithm in the following manner: a set of retrieval coefficients was associated with each measured tropopause level; these coefficients were constructed from an ensemble of temperature profiles whose tropopause pressures were restricted to a ±20 mb interval, centered about the measured point. In Fig. 6, two radar/radiometric (active/passive) retrievals, obtained with this technique, are compared with the radiometric retrieval only and with coincident radiosonde profiles. Note that the active/passive profiles improve sub-

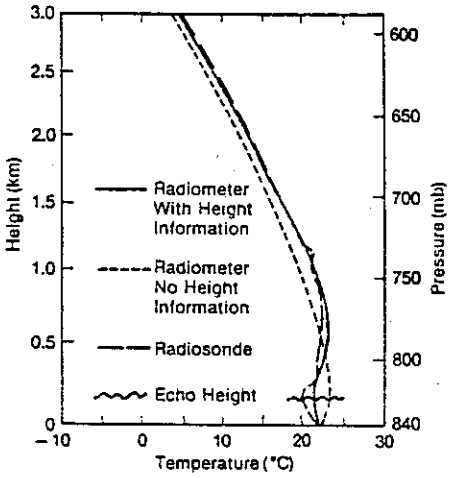

Figure 6. Temperature profile retrieved with and without radar-measured height of an inversion 6 September 1978, Erie, Colorado, compared with local radiosonde.

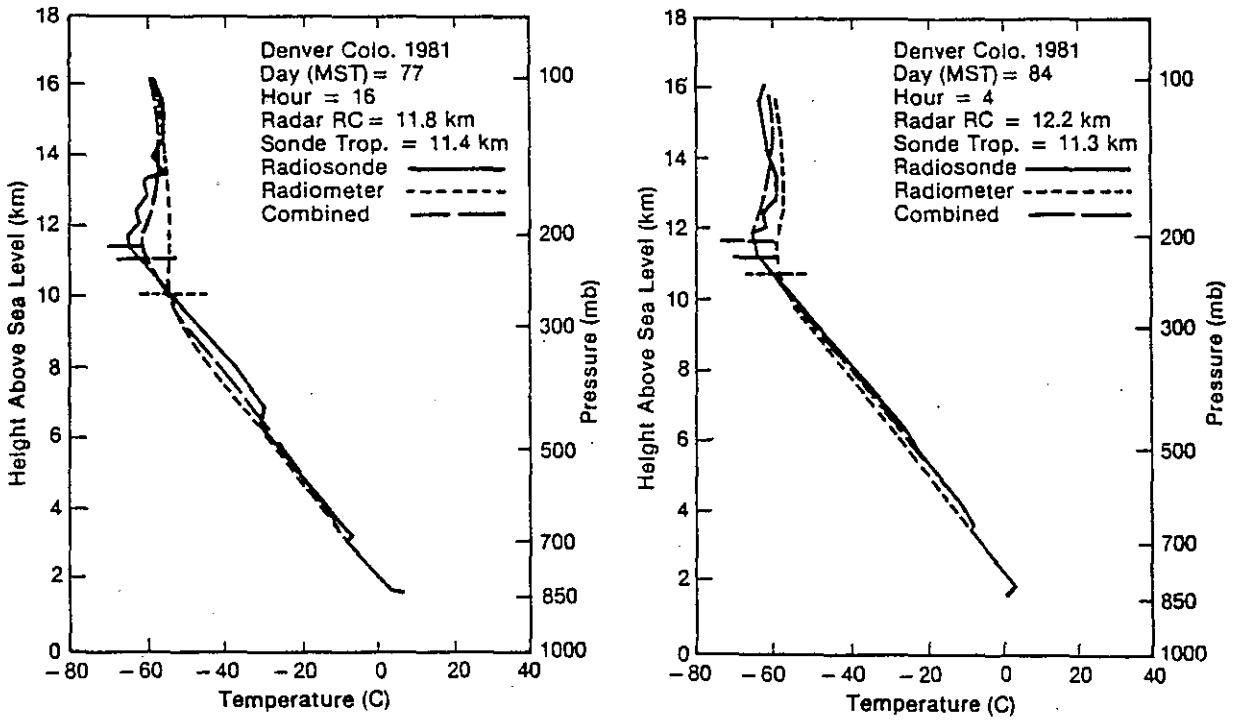

Figure 7. Temperature profiles retrieved using radiometric data only (dotted lines) and joint retrieval including VHF radar-measured height of the tropopause (dashed lines) compared with radiosonde (solid lines).

stantially in the vicinity of the tropopause, and that in both cases the improvement persists over an extended altitude range. The rms error statistics, for the 21 cases for which simultaneous radar, radiometric and radiosonde data have been compared, are shown in Fig. 6. As much as 2 K rms improvement in retrieval accuracy is achieved by the addition of tropopause height information. The heights of pressure surfaces, using profiles incorporating inversion-height correction, have not yet been made.

Although the improvement in retrieval of temperature profiles with the joint active/passive technique is evident, work remains before it is applied in a real-time operational mode. Echoes measured by the active sounder may arise from atmospheric properties different from those assumed here, hence further experience must be gained before this technique is applied with complete confidence.

3.4 NOAA Polar Orbiting Satellites

The TOVS system onboard the TIROS-N polar orbiting satellites is a third generation complement of vertical sounding instruments capable of providing complete global coverage of vertical temperature data between the surface and the stratopause and the total moisture content in that layer.

The TOVS instruments that evolved from the initial study reflect the above considerations and the experience gained as the later experiments were flown. Final design specifications represented the accumulation of knowledge up to 1976.

The TOVS consists of three instruments: (1) the second version of the High resolution Infrared Radiation Sounder (HIRS-2) originally tested aboard the Nimbus-6 satellite, (2) the Microwave Sounding Unit (MSU), which is similar to the Scanning Microwave Spectrometer (SCAMS) flown on Nimbus-6, and (3) the Stratospheric Sounding Unit (SSU) provided by the British Meteorological Office, which is a Pressure Modulated Radiometer (PMR) similar to the one flown on Nimbus-6.

The main tropospheric instrument is the 20 channel HIRS, which consists of seven temperature sounding channels in the 15 μm region, five more temperature sounding channels in the 4.3 μm region, one ozone channel at 9.7 μm, three window channels at 11.1, 4.0, and 3.7 μm, three water vapor channels at 8.3, 7.3, and 6.7 μm, and one visible channel. This instrument is supplemented in the stratosphere with the Stratospheric Sounding Unit (SSU), a three channel instrument that uses a pressure modulation technique to measure the upper atmosphere. The HIRS is also supplemented by a Microwave Sounding Unit (MSU) to help eliminate the effects of clouds and to provide a limited sounding capability in overcast regions. The MSU is a four channel instrument consisting of a window channel and three atmospheric channels. A summary of TOVS channel characteristics are given in Table 10.

When the data are received, locations based on the satellite orbit are assigned and the data are calibrated. Adjustments are subsequently made for the change in radiance with angle, the water vapor attenuation in the window channel, and surface emittance and diffraction effects in the microwave channel. Smith et al. (1979) describe the flow of data through the programs, and Phillips et al. (1979) provide additional information.

These straightforward processing procedures are followed by complex data processing algorithms which are required for soundings under cloudy conditions. Because radiation in the infrared region does not penetrate clouds, the radiation in a cloudy area is not representative of the region below the clouds. Therefore, the program first attempts to determine which areas are clear by using various tests, such as those based on known clear-air statistical relationships between channels. If cloud-free areas are not found, an attempt is made to extract clear radiances from partly cloudy values. In this process, the fact that microwave radiances are relatively unaffected by most clouds is used. If clear infrared radiances cannot be extracted, an attempt is made to produce a retrieval using only the microwave radiances. Finally, no retrievals are made if the tests for good retrievals fail. A detailed description of the entire procedure is given by McMillin and Dean (1982). Once cloud-free radiances are obtained, they are converted to brightness temperatures from which temperature profiles are determined by using the eigenvector regression described by Smith and Woolf (1976). Regression coefficients for the latitude zone containing Denver are updated weekly using colocated radiosonde data uniformly distributed over the past two weeks. Coefficients are then used for the following week resulting in an average time lag of about one and one half weeks.

Westwater et al. (1984) describes the results of a study to evaluate the relative performance of the TOVS onboard the NOAA 6/7 satellites, the Denver Stapleton Airport MWP profiler and a combination of the two. Radiosonde data for the period December

Table 10. Characteristics of TOVS sounding channels.

HIRS

Channel number	Central wavelength (μm)	Principal absorbing constituents	Level peak energy contribution (mb)	Purpose of the radiance observation
1	15.00	CO_2	30	Temperature sounding
2	14.70	CO_2	60	
3	14.50	CO_2	100	
4	14.20	CO_2	400	
5	14.00	CO_2	600	
6	13.70	CO_2/H_2O	800	
7	13.40	CO_2/H_2O	900	
8	11.10	Window	Surface	Surface temperature and cloud detection
9	9.70	O_2	25	Total ozone concentration
10	8.30	H_2O	900	Water vapor sounding
11	7.30	H_2O	700	
12	6.70	H_2O	500	
13	4.57	N_2O	1000	Temperature sounding
14	4.52	N_2O	950	
15	4.46	CO_2/N_2O	700	
16	4.40	CO_2/N_2O	400	
17	4.24	CO_2	5	
18	4.00	Window	Surface	Surface temperature
19	3.70	Window	Surface	
20	0.70	Window	Cloud	Cloud detection

MSU

Channel number	Frequency (GHz)	Principal absorbing constituents	Level peak energy contribution	Purpose of the radiance observation
1	50.31	Window	Surface	Surface emissivity and cloud attenuation determination
2	53.73	O_2	700	Temperature sounding
3	54.96	O_2	300	
4	57.95	O_2	90	

Table 10. Characteristics of TOVS sounding channels (continued).

SSU

Channel number	Wavelength (μm)	Principal absorbing constituents	Level peak energy contribution (mb)	Purpose of the radiance observation
1	15.0	CO_2	15.0	Temperature sounding
2	15.0	CO_2	4.0	
3	15.0	CO_2	1.5	

1981 to December 1982 taken by the National Weather Service at Stapleton Airport were used as "ground truth" for comparison; 460 soundings were analyzed including 216 clear, 173 partly cloudy and 71 cloudy cases. Comparisons show the profiler retrievals were more accurate than those of TOVS in the lowest 500 mb of the atmosphere, with the converse being true above that level. (Combined temperature retrievals were more accurate, in the rms sense, than either of the separate retrievals at every level from the surface to 10 mb.) The rms temperature differences for the entire data set are shown in Fig. 8. The results indicate that the remote sensing capability of ground-based radiometers can be effectively extended above 500 mb by using NOAA 6/7 satellites.

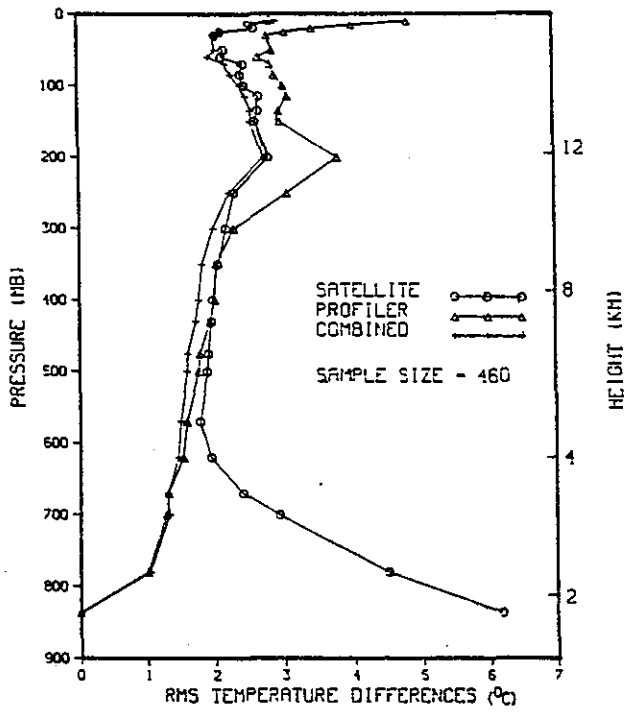

Figure 8. Rms temperature differences of radiosonde from satellite, Profiler and combined system.

3.5 NOAA Geostationary Satellites

The VAS system on NOAA's Geostationary satellites operates in the infrared. Therefore, in contrast to NOAA 6/7 it does not contain microwave channels and hence cannot routinely sound in the presence of all clouds. The VAS is a radiometer possessing eight visible channel detectors and six thermal detectors that sense infrared radiation in 12 spectral bands. A filter wheel in front of the detector package is used to achieve the spectral selection. The central wavelengths of the spectral bands lie between 3.9 and 15 μm (Table 11). Housed in the GOES satellite, VAS spins in a west to east direction at 100 rpm and achieves spatial coverage at resolutions of 1 km in the visible and 7 or 14 km in the infrared (depending upon the detector employed) by stepping a scan mirror in a north–south direction.

Designed for multipurpose applications, the VAS can be operated in two different modes: (1) a multi-spectral imaging (MSI) mode, and (2) a dwell sounding (DS) mode. Within each mode of operation there is a wide range of options including spatial resolution (7 km or 14 km), spectral channels, spatial coverage, and time frequency of observation. The mode of operation is programmed into an onboard processor from the ground through 39 processor parameters (Santa Barbara Research Center, 1978).

Table 11. VAS channel characteristics.

Channel number	Central wavelength (μm)	Absorbing constituent	Typical sounding radiance noise ($mWm^{-2}sr^{-1}cm$)	Weighting function peak (mb)	Purpose of the radiance observation
1	14.71	CO_2	0.593	40	Temperature sounding
2	14.45	CO_2	0.253	70	
3	14.23	CO_2	0.133	150	
4	13.99	CO_2	0.112	450	
5	13.31	CO_2	0.113	950	
6	4.52	CO_2	0.002	850	
7	12.66	H_2O	0.123	surface	Water vapor sounding
8	11.24	window	0.024	surface	Surface temperature and cloud detection
9	7.25	H_2O	0.082	600	Water vapor sounding
10	6.73	H_2O	0.043	400	
11	4.44	CO_2	0.002	500	Temperature sounding
12	3.94	window	0.001	surface	Surface temperature and cloud detection

The DS mode of operation permits multiple samples of the upwelling radiance in a given spectral band to be sensed by the same detector by leaving the filter position and mirror position fixed during multiple spins of the spacecraft. The DS mode of operation was designed to achieve the improved signal-to-noise ratios required to interpret the spectral radiance measurements in terms of vertical temperature and moisture structure. Spatial averaging of several 14 km resolution observations may be employed to further improve the sounding radiance signal-to-noise ratios. A summary of the VAS instrument characteristics associated with the DS mode of operation is provided by Smith et al. (1981).

The initial sounding retrieval system developed by the NOAA/NESS group and SSEC scientists at the University of Wisconsin is man-machine interactive. An operator at a Man-computer Interactive Data Access System (McIDAS) terminal can view, on a television console, visible and infrared images obtained during the DS period and select geographical positions on the image for processing vertical temperature and moisture profiles from the VAS radiances. The operator can execute programs to automatically average the data spatially for a fixed geographical area or to average a sequence of manually selected points prior to the sounding extraction process. The sounding retrieval method is the iterative inverse solution of the radiative transfer equation developed by Smith (1970). Currently, a forecast temperature and moisture field valid at 1200 GMT of each day is obtained from the National Meteorological Center (via a computer-to-computer link). This forecast is used to obtain initial profiles for the iterative solution. The same forecast is used throughout the day to ensure that diurnal variations resulting in the VAS retrievals are due solely to the diurnal variations in the atmospheric radiance to space observed by VAS. Hourly surface data can be incorporated into the retrieval process to permit computations of pressure heights and gradient winds from the VAS temperature and moisture profile data. Soundings are calculated between the surface and 10 mb from radiance data in cloud-free regions and from cloud top pressure to 10 mb in overcast regions. In overcast regions the profile below the cloud is obtained by interpolating between the cloud top and the surface. The operator selects either cloud-free or cloud-overcast 14 km fields of view for the sounding extraction. The processing system is designed to operate in real time, with soundings computed from previous scan lines as new scan lines of data are acquired. With the existing VAS data acquisition and processing system at the University of Wisconsin it is possible to provide soundings to a meteorological user at a McIDAS terminal within minutes of the radiance observation time.

On 1 July 1981, VAS, then in a trial period prior to the operational phase, made special dwell soundings for the Denver area; the weather conditions were clear. Three profiles were obtained; a typical one is shown in Fig. 9. The retrieved temperature profiles are in reasonable agreement with the radiosonde, but the satellite humidity profile, when integrated with height, yields a precipitable vapor that is 50% higher than that obtained with the profiler or the Denver radiosonde launched a few hours earlier.

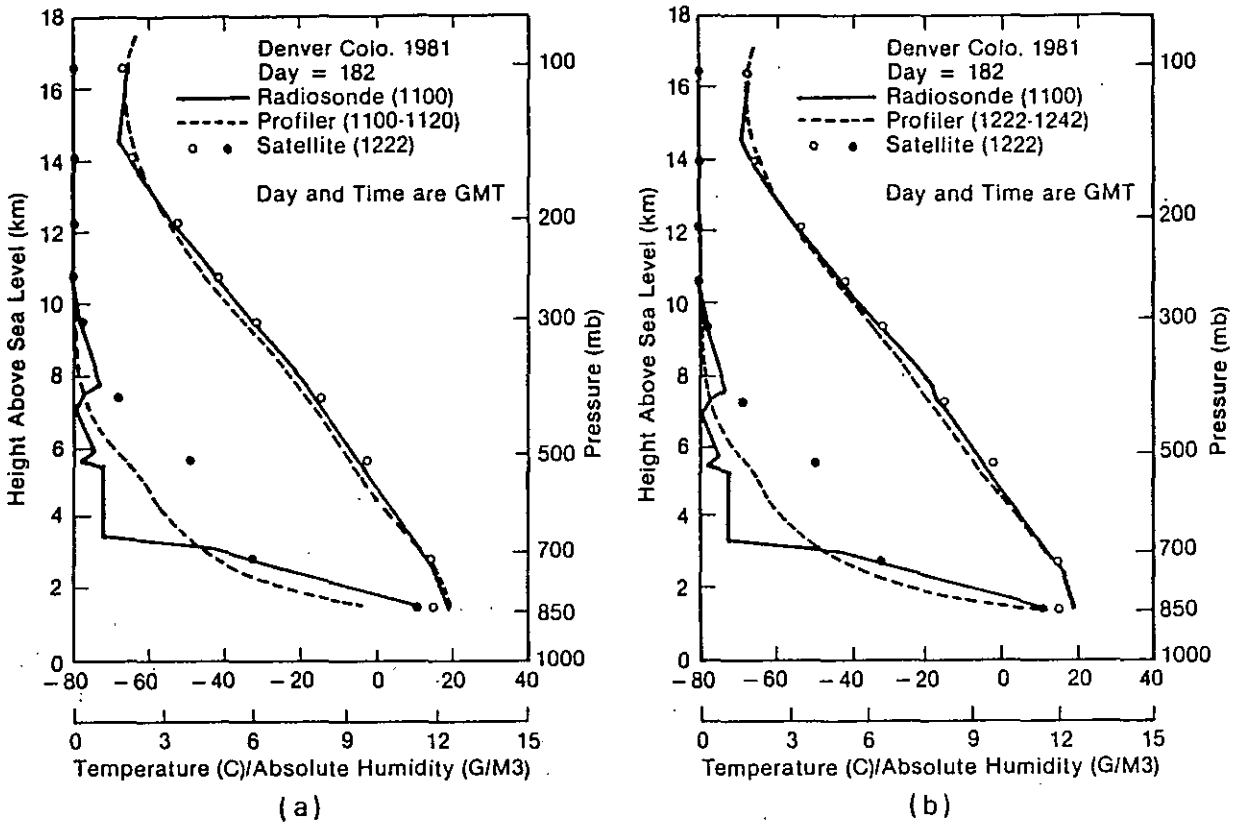

Figure 9. Comparison of a sounding taken by the VAS on GOES-5 with Profiler and Denver radiosonde profiles: (a) Profiler and radiosonde times coincident, (b) Profiler and satellilte sounding times coincident.

3.6 Lidars

The pulsed Doppler lidar is the optical analog to the more familiar Doppler radars. However, the lidar's shorter wavelength allows it to obtain a somewhat different set of information about the atmosphere, although some applications overlap those of radar. The WPL coherent infrared Doppler lidar has operated since 1981. Its features and measurements will be described, followed by some discussion of technological developments in this rapidly advancing field.

In the WPL lidar, a pulsed CO_2 TEA (Transverse Excited, Atmospheric pressure) laser emits a single frequency using an injected beam from a continuous wave (CW) CO_2 laser to define and stabilize the frequency. The wavelength is selectable from among many CO_2 laser lines in the 9–11 micrometer band, but 10.59 micrometers is normally used. The pulse is transmitted into the atmosphere through a 28 cm diameter telescope. A flat-mirror scanner on the roof of the trailer housing the lidar directs the beam to any desired direction above horizontal. The beam divergence of only 50 microradian is much narrower than radar beam widths. The lidar has no sidelobes and suffers no complications from ground clutter except for direct strikes. Maximum range in the boundary layer varies between 10 and 30 km depending on atmospheric conditions.

Aerosol or cloud particles scatter part of the light back to the same telescope. These small particles follow air motions well and give a faithful measure of air speed. The backscattered light is coherently mixed with a CW local oscillator (LO) beam in the lidar on a high-speed HgCdTe detector. This coherent detection technique (which is also used in all modern radars) provides excellent sensitivity. The heterodyne detection from the LO, which is offset in frequency from the transmitted pulse, permits measurement of the magnitude and sign of the Doppler shift of the light. The lidar is thus able to measure the radial (along-beam) component of wind as a function of range plus the range-resolution amplitude of backscatter.

The lidar uses the VAD (Velocity-Azimuth Display) technique for profiling the horizontal wind. The lidar performs range-resolved velocity measurements throughout a conical scan through 360° azimuth at a constant elevation angle of, say, 30° (Fig. 10). The VAD winds at each range have a sinusoidal pattern. The azimuth of the velocity peak gives the wind direction, and the amplitude of the peak gives the speed. Processing at WPL performs a least-squares fit of a sinusoid to the data to obtain a spatial average over turbulent eddies. A lidar could also measure the horizontal wind with only two beam directions like the microwave wind profiler, but the VAD technique is less susceptible to errors if flow is inhomogeneous.

Aerosol loading in the lowest 3 km of the atmosphere usually is sufficient for the lidar to obtain wind measurements with good signal to noise ratio (SNR). Two exceptions may occur. First, signals are sometimes weak from very clean air above a capping inversion; SNR is poor, but extra averaging can usually yield satisfactory data. Second, thick clouds or fog will block the IR radiation and prevent measurements from beyond. Obscurants like smoke may also attenuate the pulses, but to less extent in many cases than at visible

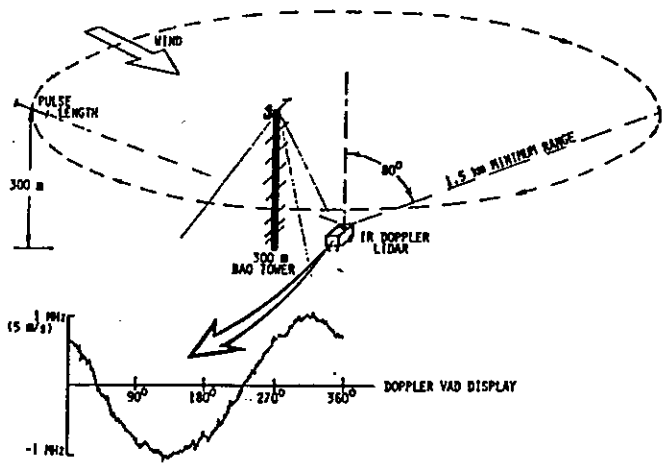

Figure 10 The VAD technique for measuring Doppler lidar winds.

wavelengths. Although the WPL lidar is not designed for all-weather operation, a Doppler lidar should be able to perform in rain or snow, although attenuation may limit the range. Satisfactory SNR from the upper troposphere is more intermittent. Aerosol loading is often quite low in certain regions, such that high pulse energies are required to adequately measure winds. However, studies performed using the WPL Doppler lidar have shown that, in many cases, thin layers of strong aerosol loading exist throughout the troposphere. Signals from these layers and from ice clouds often provide good wind measurements even under low aerosol atmospheric conditions.

A CO_2 lidar also has the capability of measuring profiles of humidity with the DIAL (DIfferential Absorption of Light) method (Hardesty 1984; Grant et al., 1987). Two wavelengths are transmitted, one on a water vapor absorption line and the other not. A measurement of the difference in attenuation combined with knowledge of the absorption cross section of water molecules gives the profile of absolute humidity. Coherent detection as used in the Doppler systems is much more sensitive than direct detection, which is limited by high detector noise. However, coherent DIAL is not as close to routine applications as is DIAL using direct detection.

The Doppler lidar is able to obtain information on wind fields beyond that measurable by radar or sodar. It can measure cloud cover and base height while it is profiling the wind. The lidar also can reveal inhomogeneous flows that might be important in tactical situations. For example, Fig. 11 shows measurements of radial velocity from an elevation scan or RHI (Range-Height Indicator) during the collision of cold-air outflows from two distant thunderstorms. In this case, the density current from the left was warmer and

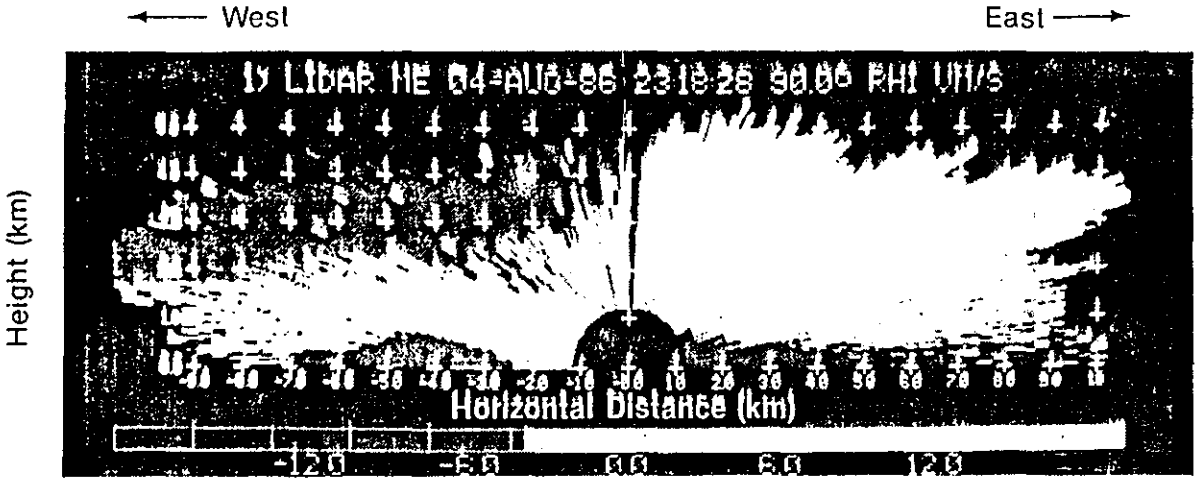

Figure 11. A 180° RHI lidar scan of the radial velocity (m s^{-1}) field at 2318 UTC. The scan clearly shows the boundary approaching from the west, forcing the old easterly outflow to rise up and over the disturbance. Negative velocities represent the wind component toward the lidar.

rode up and over the one from the right. A simple vertical profile of wind would not be representative. The lidar has also observed inhomogeneous flow fields associated with microbursts, complex terrain, developing sea breeze, lee waves in flow over mountains, frontal passage, and other instances of unsettled weather. The narrow, eye-safe beam allows distant wind measurements down to the ground that a radar cannot perform.

Doppler lidar technology is experiencing rapid improvements. Part of this progress is due to NASA's LAWS (Laser Atmospheric Wind Sounder) program, which plans to launch a Doppler lidar for measuring tropospheric winds in the late 1990's. As a research device, the WPL lidar requires an operator. However, we believe there are no fundamental limitations to engineering a turn-key system. Although many non-Doppler lidars operating within or near the visible band are not eye-safe, the energy transmitted out the telescope of the CO_2 lidar is completely safe. The Doppler lidar must have a stable frequency, including a reference against which to compare the Doppler-shifted light scattered by particles moving with the air. In the present configuration, a CW injection laser, with optical frequency locked to the peak of the gain curve at the selected line, is the fundamental reference. Its beam passes through the TEA pulsed amplifier, which emits at the same frequency, except it does pull away a bit from the injection frequency. Velocity measurements are quite satisfactory in spite of this frequency chirp, but research is in progress to reduce the chirp and improve the velocity accuracy. The local oscillator laser is locked to an electronically controlled offset of typically 20 MHz from the injection laser. The radiation scattered by particles and collected by the telescope is combined with the beam from the local oscillator on a HgCdTe detector. The coherent detection requires that the phase fronts of the signal and local oscillator beam are aligned. A small part of the outgoing pulse and the local oscillator is mixed on a separate detector. Data from this pulse monitor permit correction of residual velocity errors from the chirp. Coherent detection not only permits measurement of the Doppler shift, but it also enables sensitivity approaching the quantum efficiency limit of the detector even for weak signals that detector noise would mask.

Velocity accuracy for one pulse is typically 1 m/s. We usually perform a 3–pulse average for an accuracy of 0.5 m/s. Winds obtained from the many pulses in the VAD average out almost all of this random uncertainty plus turbulent eddies to make a highly representative measurement of horizontal wind. Tests against tower-mounted anemometers, radiosondes, and microwave wind profilers have confirmed the accuracy of the Doppler lidar (Hall et al., 1984; Lawrence et al., 1986).

A polarization technique is used to achieve the function of a transmit/receive switch. The linearly polarized light from the TEA laser is directed to the telescope by reflection at Brewster's angle. A waveplate converts to circular polarization on transmission. The same waveplate converts the received energy to linear polarization orthogonal to the laser's. The atmospheric signal thus reaches the detector, while the energy from the pulsed laser, blocked from the detector, is transmitted.

Detector output is amplified and processed with a dedicated digital processor. The detector output is separated into in-phase and quadrature components (to get sign and magnitude of the Doppler shift). Each is digitized at 10 m range intervals. The processor

computes the time-lagged autocorrelation of the signal over the Doppler range gate of usually 300 m. We typically use 4 lags in this polypulse pair processor. Pulse averaging is performed when desired on these autocorrelations. A Fourier transform on the result gives the frequency spectrum, and a peak detector algorithm determines the Doppler shift. Data are displayed in real time on color terminal and recorded on magnetic tape for postprocessing and further analysis.

A difference between radar and lidar processing is the time required for the scatterers to move a substantial portion of the wavelength for a good Doppler shift estimate. Radars compare signal changes between pulses for the measurement, whereas the lidar must do this as a pulse sweeps past the target.

System sensitivity, which determines the maximum range for good velocity measurements, depends on several factors. SNR increases with pulse energy and the number of pulses averaged. The system range function is relatively independent of range R within the near field ($R < 10$ km in the WPL system), then declines as R^{-2}. Two-way losses in the boundary layer from gaseous absorption by the 10.59 micrometer CO_2 line and by the water vapor continuum are typically 1 dB/km, less in winter and more in humid, warm conditions. This absorption is why a 10 dB decrease in pulse energy will reduce the maximum range in the boundary layer by only a factor of 2 (roughly). The effective detector quantum efficiency, which also depends on the match between signal and local oscillator phase fronts, is another factor. The aerosol backscatter cross section, which can vary strongly in the vertical and with time, is a primary factor for sensitivity.

3.7 Sodars

A major advance in sodar technology was made by McAllister (1968) when he developed a device to display acoustic echoes from the atmosphere similar to devices used to display sonar echo data from the ocean. In most such devices, a pen is mechanically drawn across a specially treated paper, with each traverse corresponding to a period of interest beginning at the time of the transmitted sound pulse. After each trace is written, the paper advances in time to draw the subsequent trace adjacent to the previous one. From such a display of echo returns, a time-height record of the atmospheric structure moving through the antenna beam is constructed. The height (or range) of echoes displayed across the paper is deduced by knowing the transmission time and the average speed of sound. More recently, microprocessor technology, color graphics terminals, and dot matrix printers have provided alternatives to the original analog facsimile displays. A detailed treatment of acoustic remote sensing is given by Neff and Coulter (1986).

Because of the relatively slow speed of sound compared with that of electromagnetic waves, instrumentation for and processing of acoustic data are relatively simple. Therefore, acoustic techniques are relatively inexpensive, and sophisticated analysis of the data is not usually required.

Most components for monostatic sodar are readily available. The parabolic reflector of a searchlight combined with a foam-lined acoustic shield can provide an effective antenna with a conventional compression driver serving as a transmitter/receiver. Display devices

can be adapted from standard sonar facsimile recorders. Digital processing for Doppler analysis is now easily available with inexpensive microprocessors. The sound frequency used in commercial sodar is around 2 kHz. (Minisodars operating at around 5 kHz are being used for short–range profiling by a few investigators.)

Sodars can use either of two geometrical arrangements. The first, called monostatic, uses a collocated transmitter and receiver. In this mode, only the temperature spectrum contributes to the backscatter and hence researchers use this arrangement to infer the qualitative nature of the temperature profile. The second arrangement, consisting of separated transmitters and receivers, is referred to as a bistatic system. This mode provides signals that are scattered from small-scale velocity fluctuations as well as from temperature inhomogeneities. This mode of acoustic sounding is unique among remote-sensing devices insofar as it is the only remote-sensing method directly sensitive to the small-scale velocity field. Various bistatic arrangements can provide a picture of the vertical distribution of turbulence as well as better signals for Doppler wind estimates when the temperature lapse rate is close to adiabatic.

Doppler sodars are used primarily to obtain estimates of wind speed by analysis of the frequency content of the detected signal. Determination of the total wind vector in general requires the use of three transmitter-receiver combinations, each sensing a different component of the wind. This requirement can be accomplished in two basic ways: triple monostatic and bistatic. The triple monostatic system features three antennas, usually collocated, which point at different azimuth and elevation angles in order to obtain the necessary wind components. The bistatic system utilizes two separated receiver-transmitter links along with a single (usually vertically pointing) monostatic transmitter-receiver. These links can be established by using either a single transmitter and two separated receivers, which detect the signal scattered at different directions from the single transmit beam, or a single central receiver (the same as the monostatic receiver) and two separated transmitters.

Signal processing usually proceeds as follows. The received signal is protected from the transmit pulse by a transmit-receive switch, which turns on the receiver only after the transmit pulse has ended. The signal is then preamplified, either at the receiver electronics or at the receiver antenna, to decrease the effects of electrical line noise. This gain usually increases with time to compensate for attenuation and the spherical spreading of the scattered acoustic energy. Within the receiver electronics an envelope detector provides an estimate of the signal amplitude, and a quadrature detector detects the out-of-phase and in-phase components of the signal. The signal may be heterodyned to a lower frequency for digital analysis at reduced sampling rates. The signals are then transmitted to a computer that analyzes and calculates the Doppler shift which in turn is related to the wind speed.

The two methods for wind-speed determination have enough differences that a comparison of advantages and disadvantages is important. A significant advantage of triple monostatic systems is that geometrical considerations are minimized: the derived velocity for a given frequency shift is independent of height. The bistatic system requires significant geometrical corrections. In addition, the ability to locate the three antennas at one

point enhances the convenience and mobility of triple monostatic systems, whereas bistatic systems usually require 100- to 300-m baselines (for 2 kHz sodars) with cabling to match. Also, if there is sufficient return from temperature fluctuations throughout the probing range, the triple monostatic system may be able to achieve greater heights because of the coincidence of the transmit and receive beams. An additional disadvantage of the bistatic system is its increased susceptibility to ground clutter because of refraction and reflection of the broad-beam transmit pulse from low objects. Reflections from solid objects appear as bands at a constant height. Such effects can be particularly pronounced in very stable conditions when sound can be strongly refracted toward the ground.

On the other hand, the triple monostatic system requires heavy shielding on all three antennas, two of which are not pointing vertically and are thus more susceptible to environmental noise contamination. More important, perhaps, is the fact that the triple monostatic system depends upon estimates made at three different positions in space to derive the velocity and turbulence estimates. This can be a severe limitation even for mean wind estimates in situations where conditions are not homogeneous—over complex terrain or land-water interfaces, for example. Finally, because the monostatic system is dependent upon C_T^2 alone for its signal source, its signal may be smaller than the bistatic signal, particularly when the atmosphere is adiabatic.

Both systems have a similar, less severe problem in that they transmit alternately among the three antennas. (This means of transmission may not be a necessity for the triple monostatic system if the beam patterns of the three antennas do not interfere with one another.) Thus the individual components of the wind are not derived from the same volume of air. This problem can be overcome for both systems by transmitting at different frequencies from each transmitter and analyzing the signal near each transmit frequency for the different components.

Most commercial and research systems have incorporated some means for estimating the reliability of a given frequency shift, or wind estimate. Details differ in implementation but usually involve some estimate of the signal-to-noise ratio (S/N) and absolute signal level during data collection.

The limiting factor in velocity determination with sodar is usually the amount of environmental noise included in the signal. Most analyses of the effect of noise upon Doppler signals assume a white noise spectrum; however, this is probably only rarely encountered. Reflections, birds, and insects produce limited-bandwidth signals, which affect the signal in different ways depending upon their type and proximity. Airplanes, a constant nuisance, produce a wider-band signal. Thus, it is important to sample the background noise under varying circumstances and to produce noise spectral estimates.

The effect of noise is usually to bias the measured Doppler frequency toward zero; that is, the effect of white noise on many full-spectrum techniques if

$$\delta f_m = \delta f\{(S/N)/[1 + (S/N)]\} \tag{1}$$

where δf_m is the measured value of δf in the presence of noise. The degree of applicability of Eq. (2) depends on the analysis technique and the spectral characteristics of the noise.

One of the consequences of noise on Doppler wind measurement is the limitation it imposes on the height range of the sodars. In most research and commercial 2 kHz versions of the instrument, the height range of maximum reliability is 500 m. (Depending on atmospheric conditions the range at times extend to 1.0 km.) This limitation is imposed primarily by the wind noise at the antenna aperture which is amplified along with the signal as it "ramped" to compensate for the inverse square loss. This S/N limitation is exacerbated by the fact the day-time C_T^2, responsible for the backscatter of sound, drops rapidly with height. The attenuation in the backscatter signal is also a function of humidity and is strongest in the range from 20–60% RH. However, between 50 and 500 m, the sodar can be designed to perform reliably. The height range for the 5 kHz sodar is narrower, 10–100 m; although limited, it nicely complements the range of the 915 MHz Boundary Layer Profiler and merits consideration in combined remote profiling systems.

4. NEW SYSTEMS

In addition to the proven technologies discussed in Chapter 3 we need to consider some new systems proposed in recent years. These concepts have particular relevance to RAPS because they are potentially more compact and possibly more reliable. All the concepts described in this chapter are experimental systems that need to be further developed and field tested; many of them represent small variations of proven ideas, others are novel applications of established technology.

4.1 Imaging Doppler Interferometer (IDI)

The IDI technique first proposed by Adams et al. (1985) measures winds from the complex cross spectrum of signals observed at two receivers spaced distance d apart, from scatterers irradiated by a pulsed Doppler radar. The horizontal wind is inferred by tracking these scatterers as they move through the sampling volume. While any of the pulsed Doppler radars described in Chapter 3 can be adapted for this purpose, the IDI technique does not require narrow beams and therefore large antennas. The receiver spacing, d, could be of the same order as the wavelength (0.75 m for a 404 MHz radar) so that a transmitter-receiver array measuring 1.5 m × 1.5 m, with a beamwidth of 30 degrees can be designed to easily fit on top of a trailer or van (Lataitis, 1989). Small

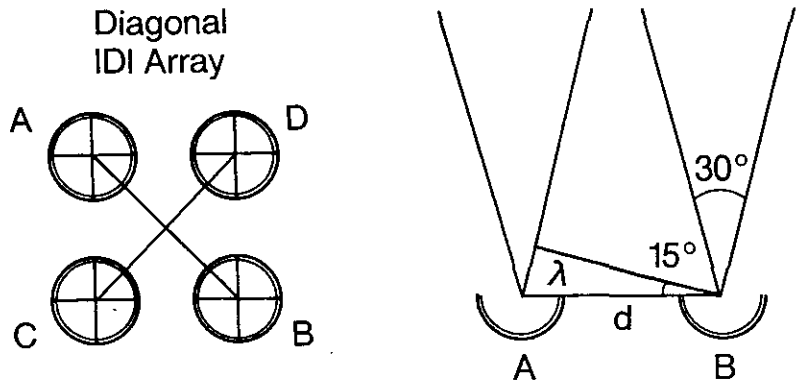

Figure 12. Diagonal array for a roof-top mounted IDI antenna.

antenna size mandates higher transmitter power to maintain accuracy in wind profiling (500 watts for 3 km range compared with 5 watts in the three-beam pulsed Doppler radar). Lataitis et al.'s (1989) specifications for a 404 MHz IDI system with 300 m range resolution and 10 km range for the same size antenna list 10 kW transmitting power. In a diagonal four-antenna configuration (see Fig. 12), all four antennas would operate as transmitter while each set of diagonal antennas would serve as receiver pairs. For a 30 degree beam width, the maximum separation between receiver points would be $\approx 3\lambda$ to keep the phase delay within 2π which, for λ = 0.75 m, would be 2.25 m.

The IDI method was first applied to ionospheric measurements in the early 1970's (Woodman, 1971). It wasn't until the mid 1980's that it was used for mesospheric and stratospheric wind measurement and only very recently (Volek, 1989) for tropospheric wind profiling. IDI is still very much an experimental technique unproven in the troposphere and inconclusive at best in the mesosphere and stratosphere. However, it is potentially capable of revealing details of the wind field not attainable by the three-beam Doppler method.

In contrast with the Doppler method, the IDI technique requires the existence of persistent scattering centers in the radar volume with differing radial velocities. In the troposphere these are likely to be patches of turbulence that are remnants of thermal plumes. To obtain an estimate of the wind, a number of these patches need to be located in the radar volume and tracked as they move through the volume. Scatterers can be identified by their differing radial velocities which appear as discrete peaks in the Doppler spectrum. The greater the number of scattering centers that can be identified and tracked, the more reliable the wind estimate. Short dwell times are needed to minimize errors in the position of the scatter caused by motion during the measurement time. The resulting SNR can therefore be very low. Some improvement can, however, be realized by using multiple interferometers to identify a single scatterer. The scatterers also need to persist for a sufficiently long time that they can be tracked and a wind speed inferred from their motion. The number and lifetime of these tropospheric scatterers, as well as the ability of an optimized IDI system to detect them, is currently unknown.

The theoretical aspects of IDI are discussed in the report by Lataitis et al. (1989). Extraction of winds from cospectra generated from the gated Doppler returns at the two receivers involves extensive data processing. To summarize the approach briefly, we assume that the distinct peaks appearing in the cospectrum are associated with "scattering centers" in the radar volume. The frequency of this peak gives the radial velocity of the scatterer. The corresponding phase of the cospectrum can be related to the arrival angle of the scattered field which locates the scatterer in the radar volume. A sequence of cospectra can then be used to track the scatterers which yield a map of their positions in the radar volume versus time. Assuming these scattering centers are passive additives that are merely advected by a bulk flow, the mean wind velocity can potentially be retrieved as can sub-volume details of the air motion.

A related technique to the IDI is the spaced antenna (SA) method. It is discussed in detail by Lataitis et al. (1989) and only briefly mentioned here. It can also be implemented using the antenna configuration shown in Fig. 12. In contrast with the IDI technique, which uses cospectra generated from signals at various receiver pans to obtain wind information, the SA method relies on the temporal cross–correlation functions generated from the various pairs of received signals. This method is based on the direct relation between the evolution of the backscattered diffraction pattern on the ground and the evolution of the turbulence in the radar volume. More precisely, if we invoke Taylor's hypothesis and assume that changes in the refractive index field within the scattering volume are simply the result of a frozen refractive index field being advected by a mean wind V, then the evolution of the backscattered diffraction pattern will also consist of an unchanging pattern moving, however, with velocity 2V. The delay to the peak of the various cross–correlation functions can then be used to infer V. The full correlation analysis (FCA) used in analyzing the various cross–correlation is described in detail by Briggs (1950, 1984). The interferometric aspect of this technique arises when the phase or the cross–correlation is used to inter the mean vertical wind (Rottger and Ierkic, 1985).

On advantage to the SA technique over the IDI method is that it is more of a proven technology and has been successfully applied in the troposphere (e.g., Rottger and Czechousky, 1980) whereas initial attempts with the IDI in the troposphere were inconclusive (Volek, 1989). Another relative advantage is the lower power requirements; our estimates indicate up to a factor of ten difference. On advantage of IDI is its potential for probing sub–volume details of the wind field.

4.2 Acoustically-Enhanced Profiler (AEP)

The acoustically-enhanced approach differs from the single beam RASS systems described in Chapter 3 in that it uses the speed of the propagating sound waves measured along four inclined radar beams to compute both the horizontal wind components and temperature. The measured speed of the propagating wave C_m is the algebraic sum of the sound speed in still air, c_o, and the wind component in the radial direction, V_r, along the beam so that if two of the inclined beams are pointing in opposite directions in the azimuth, say east and west, we have

$$(C_m)_E = c_o + (V_r)_E = c_o + w\cos\phi + u\sin\phi \tag{2}$$

$$(C_m)_W = c_o + (V_r)_W = c_o + w\cos\phi - u\sin\phi \tag{3}$$

where w and u are the vertical and east-west wind components respectively, and ϕ is the inclination of the beam from the zenith (Fig. 13). Similarly for the north and south beams, designating v for the north south wind component,

$$(C_m)_N = c_o + (V_r)_N = c_o + w\cos\phi + v\sin\phi \tag{4}$$

$$(C_m)_S = c_o + (V_r)_S = c_o + w\cos\phi - v\sin\phi\ . \tag{5}$$

At $\phi = 30°$ we have $\cos\phi = 0.87$ and $\sin\phi = 0.5$ and therefore;

$$u = [(C_m)_E - (C_m)_W] \tag{6}$$

$$v = [(C_m)_N - (C_m)_S] \tag{7}$$

$$c_o = \frac{1}{2}[(C_m)_E + (C_m)_N - 1.74w] \tag{8a}$$

$$= \frac{1}{2}[(C_m)_N + (C_m)_S - 1.74w] \; . \tag{8b}$$

We have assumed here that the wind and temperature fields are horizontally homogeneous, and to the extent that this condition is not met, an error corresponding to their horizontal variability can be expected in the resolved wind components. But the w component does appear as a contamination in c_o and consequently in the estimated temperature (as in the conventional RASS) and should be removed by time averaging the results or measuring w separately with a vertical beam. The redundancy in the c_o measurement would serve as a check on data quality.

The advantages of this method over the conventional UHF profiling are:

(1) Freedom from errors due to ground clutter which can degrade measurements at closer ranges.

(2) Freedom from sensitivity to hydrometeors and moving objects.

(3) Reliable wind measurements even in the absence of refractive index variations.

(4) Freedom from contamination from w in the horizontal wind measurements.

(5) The same acoustic antennas that serve as acoustic sources for RASS can be used as antennas for a mini Doppler sodar providing wind information below 100 m.

Preliminary tests conducted by Peters (1989) indicate that winds derived from a two beam (30 degree off-zenith) system can provide more accurate winds down to lower heights (50 m) than winds derived from clear-air returns from velocity turbulence alone. The 915 MHz profiler system can easily be adapted for this purpose with switchable antennas small enough to be transportable.

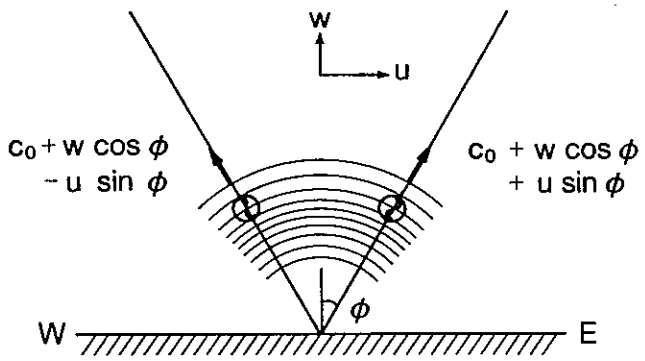

Figure 13. Speed of sound measured along two Profiler beams in an acoustically enhanced Profiler system.

4.3 High-Resolution Interferometer Sounders (HIS)

The High-resolution Interferometric Sounder is a Michelson interferometer developed primarily as an aircraft prototype of a new generation satellite sounder (Smith et al., 1983; Revercomb et al., 1988). It operates in the infrared region between 600 and 2600 wavenumbers (i.e., 16.8–3.8 microns) using three detectors to divide the spectrum into three bands: band 1 (600–1080 cm^{-1}), band 2 (1080–1830 cm^{-1}), and band 3 (2000–2600 cm^{-1}). The spectral resolution of the raw data is about 3000/1. The data are processed by Fourier transformation of a truncated and apodized interferogram yielding a spectral resolution of about 0.5 cm^{-1}, 1.5 cm^{-1}, 1.5 cm^{-1} for bands 1, 2, and 3 respectively. When operating in the upward-looking mode at Denver Stapleton, complete spectra were achieved every four seconds. Two blackbodies, an Eppley cavity heated to 300 K and a bath of liquid nitrogen at 77 K, were used to calibrate the measurements once per minute. The sky, at local zenith, and the blackbody references were viewed using a scene switching mirror. For atmospheric profiling purposes, the calibrated spectra, produced every four seconds, are averaged over five minute time intervals with the mean and standard deviation spectra being output for use in sounding and trace gas concentration retrievals.

An example of a radiance spectrum observed with the HIS is shown in Fig. 14 along with a spectrum calculated using a regression atmospheric transmission model based on FASCODE (Clough et al., 1986) and a CLASS sounding of temperature and water vapor. As can be seen, there is extremely good agreement between the spectral features shown in the observed and calculated spectra, the minor exception being in the "window" region between 800 and 1000 cm^{-1} (panel 1) due to emission by Freon 11 and 12 which was not included in the FASCODE calculation. The mean difference and standard deviation of all the observed and calculated spectral radiances achieved during the entire GAPEX period is shown in Fig. 15. Because the observed spectra are believed to be accurate to better than 0.5%, the differences shown are due primarily to errors in the FASCODE spectroscopy with second order differences being due to time and space variability in the atmospheric temperature and water vapor.

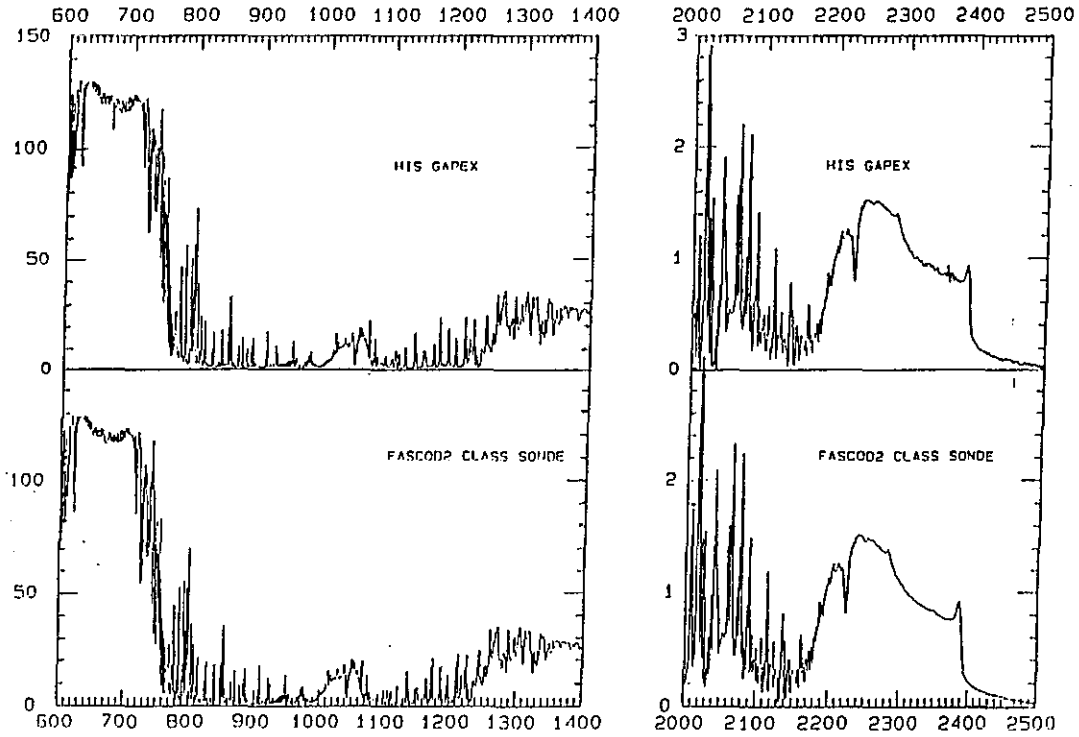

Figure 14. Comparison between downwelling radiance spectra observed by the HIS and calculated using a CLASS temperature and water vapor sounding. (After Smith et al., 1989).

For the retrieval of atmospheric temperature and dewpoint temperature profiles from the HIS spectra, a linear simultaneous statistical inversion method is used. The covariance matrices of temperature and dewpoint utilized in this solution were obtained from the same ten year climatological sample of radiosonde observations at Denver (Westwater et al., 1985) used for the MWP retrievals. Figure 16 shows a plot of the 500 mb geopotential height derived from the HIS temperature and water vapor profile retrievals as compared with the CLASS, standard NWS radiosonde observations, and the MWP. The rms difference between the HIS and the CLASS is only 12 meters. For comparison, the MWP comparisons with CLASS provide an rms difference of 17 meters. Geopotential height profiles derived from HIS are expected to be more accurate than those from the MWP

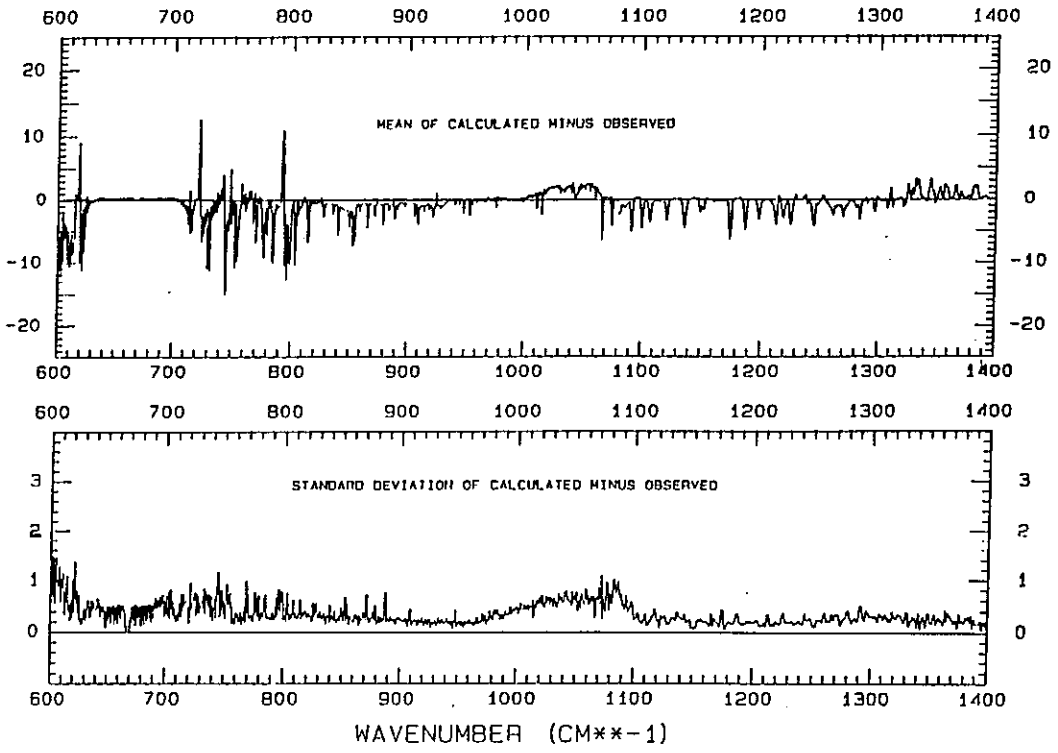

Figure 15. Statistical comparison between calculation and observation for a subset of the GAPEX soundings. (After Smith et al., 1989).

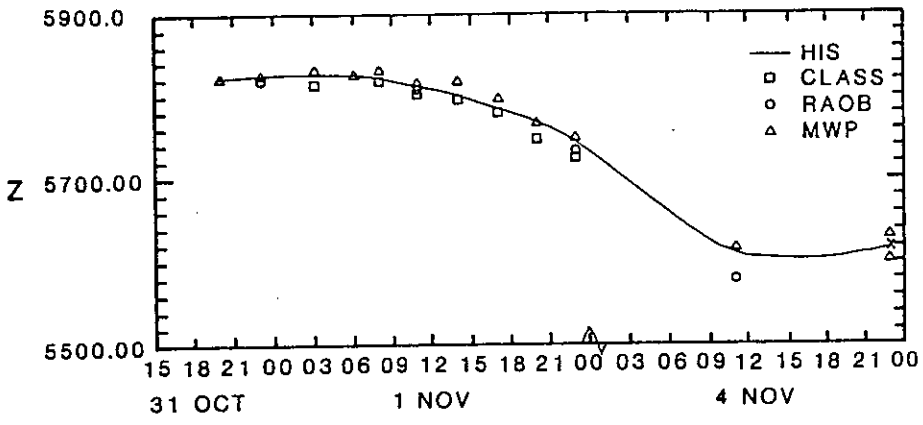

Figure 16. Comparison of 500 mb geopotential height (meters ASL) as measured by four independent measurement systems. The solid curve is from the High resolution Interferometer Sounder (HIS). (After Smith et al., 1989).

because of the much larger number of temperature and water vapor sensitive sensor channels.

4.4 Autocorrelation Radiometer (CORRAD)

The K-Band Autocorrelation Radiometer (CORRAD) built by The Microwave Remote Sensing Laboratory at the University of Massachusetts at Amherst (Ruf and Swift, 1988) performs the necessary spectral measurements through a synthesis of techniques developed for correlation radiometry and optical Fourier transform spectroscopy. Correlation radiometers are most commonly used to cross-correlate spatially separated radio telescopes for interferometric synthetic aperture imaging (Kraus, 1966). They perform the multiplication and expectation operations required of a cross correlator on two broadband signals. Optical Fourier transform spectroscopy determines the power spectral density of a signal in the optical frequency range indirectly, by measuring its autocorrelation function.

The advantage of an autocorrelation approach to spectral imaging lies in the bandwidth, B, and integration time, T, available for each measurement. The signal-to-noise (SNR) performance of most radiometers (ratio of the mean to the standard deviation of the measured system brightness temperature) is given by

$$\mathrm{SNR} = K(BT)^{1/2} \tag{9}$$

where $K \approx 1$ is proportionality constant determined by the radiometer hardware specifics. The bandwidth and integration time available for the three radiometer systems discussed above, and the resulting SNR performance, is summarized in Table 12 for the case of a total frequency range B_{TOT} which is to be resolved into N adjacent frequency bins during a time T_{TOT}.

In Table 12, the worst case performance by the autocorrelation radiometer (with serial time delay sampling) is as good as a bank of N total power radiometers and better than the single-stepped frequency radiometer. This advantage should be qualified, however, by noting that the Fourier transformation required to recover the brightness temperature spectrum from the autocorrelation measurements degrades the SNR of the transformed data by $N^{-1/2}$ relative to the original data (Ruf, 1987). This degradation can be viewed as a root-sum-squared accumulation of measurement noise during data processing. The discrete Fourier transformation at each frequency is a weighted linear combination of the individual data points. If the measurement noise associated with each point is modeled as independent additive Gaussian noise, then the standard deviation of the linear combination is the weighted root-sum-square of the individual standard deviations.

If the brightness temperature is the desired end product of the measurements, then the performance of the autocorrelation radiometer becomes comparable to that of the stepped frequency radiometer if its time delays are sampled serially and are comparable to the total power radiometer bank if they are sampled in parallel. Preliminary investigations

Table 12. Radiometer SNR comparison.

			Autocorrelation	
	Total power	Stepped frequency	Parallel*	Serial†
Bandwidth (B)	B_{TOT}/N	B_{TOT}/N	B_{TOT}/N	B_{TOT}/N
Integration time (T)	T_{TOT}	T_{TOT}/N	T_{TOT}	T_{TOT}/N
Relative SNR of raw data‡	$N^{-1/2}$	N^{-1}	1	$N^{-1/2}$
Relative SNR of brightness temperature▪ (after Fourier transform)	$N^{-1/2}$	N^{-1}	$N^{-1/2}$	N^{-1}

*All time-delay measurements were made simultaneously.
†Time delay measurements were made consecutively.
‡ $|(BY)/(B_{TOT}T_{TOT})|^{1/2}$.
▪ Same as raw data for total power and stepped frequency radiometers $|(BY)/(NB_{TOT}T_{TOT})|^{1/2}$ for autocorrelation radiometers.

into a formulation of the integral inversion problem with respect to the autocorrelation function [i.e., the Fourier transformation of (1)] suggest that the degrading transformation from measured autocorrelation samples to derived brightness temperature spectrum may be avoidable. Such a formulation could recover the SNR advantage possible with an autocorrelation radiometer.

A time series of CORRAD autocorrelation datasets was taken at the National Weather Service field station in West Palm Beach, Florida on 19 and 20 January 1987. A full set of time delay measurements, requiring about 8 min, was made at 10 min intervals near sunrise and sunset and at one-half hour intervals throughout the day. A complete report of the water vapor and liquid water estimates made from this data is available from Ruf (1987). One particular series of two consecutive profiles is shown in Fig. 17 as an example of the potential meteorological utility of CORRAD. The datasets were measured at 1629 and 1716 EDT on 20 January 1987. A heavy afternoon shower occurred from 1655 to 1705 EDT. The latter profile is significantly depleted of water vapor above 1.0 km. This demonstrates the potential CORRAD has for tracking dynamic weather conditions.

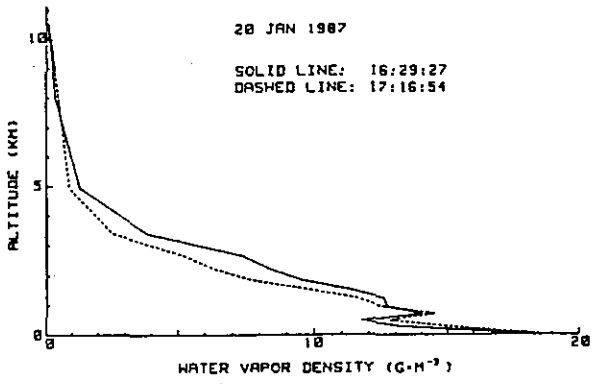

Figure 17. CORRAD profiles before and after rainfall. Heavy afternoon showers occurred from 1655 to 1705 EDT. Note the depletion of water vapor after the rains above the cloud layer (1 km altitude).

4.5 High pulse rate CO_2 Doppler lidar

Existing CO_2 Doppler lidars are in general bulky, labor-intensive, and expensive. However, Doppler lidar technology is rapidly advancing toward systems that will be compact and robust. WPL and Colorado State University through funding from the Army Research Office are attempting to incorporate a commercially available TEA laser into a lidar system instead of a custom laser as in the WPL research Doppler lidar. The development includes experimental confirmation of the purity and stability of the frequency of the laser, which the manufacturer claims should be suitable. The laser is expected to easily supply 100 mJ pulse energies at 100 Hz pulse rate. The volume, cost, and power requirements are much less than WPL's 1 J laser, although average powers are comparable. If the laser meets expectations, it could be the heart of compact, turnkey system using established technology.

4.6 Pulsed waveguide laser

RF-excited waveguide CW CO_2 lasers are very compact and efficient. They have proven hardy in applications such as measurement of air speed of high performance planes using an onboard system viewing perhaps 100 m ahead, which is outside the envelope disturbed by the aircraft. Recent developments have increased the output energy of these sources when operated in a Q-switched (pulsed) mode.

Simulations at WPL show potential for a Q-switched waveguide laser for velocity measurements in the lower 3 km of the atmosphere. The envisioned system has modest pulse energy but very high pulse repetition frequency (PRF), relying on extensive pulse averaging to reach adequate SNR. The pulse length is also much shorter than WPL's current large system, allowing better spatial resolution. Research is planned in an attempt to reach these pulse energies while maintaining frequency purity. Research is also needed to optimize processing for high data rates when the SNR for individual pulses is low.

One advantage of the high-PRF lidar is averaging of speckle noise. The amplitude of backscatter measured by coherent detection from randomly positioned particles has a standard deviation equal to the mean, even at high SNR. Because speckle-generated uncertainties in backscatter measurements are efficiently averaged, a high PRF lidar sys-

tem is highly promising for lower tropospheric water vapor profiling using the DIAL method (see Section 4.10 for a more detailed discussion of CO_2 DIAL lidar). In principle, a single instrument could provide simultaneous measurements of both wind speed and water vapor concentration.

4.7 Solid state lasers

Coherent operation of a 1.06 micrometer wavelength Nd:YAG laser in a lidar configuration was demonstrated at Stanford University (Kane et al., 1987) and improved at Coherent Technologies, Inc., in Boulder, Colorado. The system uses a MOPA (Master Oscillator, Pulsed Amplifier) configuration, which is simpler than injection locking. The pulse is generated in a multi-pass slab amplifier that is tiny compared with CO_2 lasers. The backscattered signal from the telescope is fed into a single-mode optical fiber, and then mixed in a fiber coupler with the local oscillator radiation from a connecting optical fiber. This is a miniature, robust method compared with the lenses and beams used for the coherent joining of signal and local oscillator in CO_2 lidars.

The advantages of the solid state technology include low maintenance, compactness, and good efficiency. This laser does not have gas lifetime problems like the CO_2 laser. However, the flashlamp pump of the laser has a finite lifetime and requires occasional replacement. It is quite likely that even this maintenance task can be eliminated by using laser diode prompting to attain complete solid state capability. The short wavelength from such a system inherently has the capability of providing better spatial resolution than the longer CO_2 wavelengths without compromising velocity accuracy. The main disadvantage of the Nd:YAG is that a practical system at this wavelength is not eyesafe. This work has demonstrated that Doppler velocities can be measured with a solid state laser.

Solid state lasers operating far enough in the infrared to be eyesafe are now commercially available. A leading example is Ho:YAG at 2.1 micrometer wavelength. It is possible that Ho:YAG will eventually become the ideal laser for Doppler lidar measurements in the 300 m to 10 km range.

4.8 CW Doppler lidar

The earliest Doppler lidars were CW CO_2 systems using focusing to define the measured volume. The minimum range is a few meters, but the maximum range is typically about 500 m, because the length of the resolved volume is a rapidly increasing function of R. This technology by itself is not adequate even for the tactical goal. However, a pulsed CO_2 Doppler lidar has a minimum range of the same order as the maximum range of the CW lidar. It may be reasonable to build a hybrid system for profiling from 10 m to 3 km that would share telescope, scanner, data acquisition, detector, and some other components between CW and pulsed Doppler subsystems.

Lidar technology is younger than radar and sodar technology, but has advanced more rapidly. Although Doppler lidar is not as close to operational implementation as microwave wind profilers and Doppler acoustic sounders, we expect the gap will close during the next 5–10 years.

4.9 Raman lidar

Foremost among the lidar techniques available for measuring vertical moisture profiles in the first 10 km of the atmosphere is the Raman lidar operating at 355 nm described by Melfi and Whiteman (1985). Experiment results show good agreement with direct measurements, but only at night. Its time resolution is very good (2 min) and so is its range (4 km). Its disadvantages, in addition to not being useful for daytime use include coarse vertical resolution (100 m) and the large size of telescope needed.

Raman scattering is a very weak molecular-scattering process. It is scattering whose wavelength is shifted from the incident radiation by a fixed amount associated with rotational and/or vibrational-rotational transitions of the scattering molecule. As such, the shift in wavelength from the laser wavelength is characteristic of specific atmospheric molecules. Raman scattering in the atmosphere has been observed from nitrogen, oxygen, water vapor, carbon dioxide and a number of other minor species. Melfi (1972) has shown that the ratio of the Raman-scattered signal for the water-vapor shifted line to the signal from nitrogen is, to a good approximation, proportional to atmospheric water-vapor mixing ratio. The design of the lidar takes these factors into account.

The lidar consists of a frequency-tripled Nd:YAG laser (wavelength—355 nm) whose optical axis is aligned parallel with the axis of a 1.5–m–diameter Cassagranian telescope. Both the telescope and laser are mounted in an environmentally controlled mobile van and are pointed vertically through a hatch in the van's roof. As the laser pulse propagates up through the atmosphere, it is scattered by atmospheric molecules and aerosols. Most of the scattered radiation is at the laser wavelength (Rayleigh and Mie scattering). A small amount is scattered at the shifted Raman wavelengths. The telescope collects the radiation that is scattered back toward the system. The collected radiation is spatially filtered by a field stop and divided by a beam splitter into two channels. One channel has a narrow-bandpass interference filter centered at the Raman-shifted wavelength due to water vapor (wavelength—406 nm) and the other has a filter centered at the Raman wavelength due to nitrogen (wavelength—387 nm). The filters serve to select the Raman scattering of interest, to reduce the sky background radiation, and to block the strong backscattered radiation at the laser wavelength. A photomultiplier is used in each channel to detect the radiation passed by the respective filter. The signal from each photomultiplier is amplified by an external (×10) amplifier whose 1–MHz electrical bandpass reduces high-frequency noise. After amplification, each signal is digitized at a 10–MHz rate (altitude bins every 15 m). During the experiment, the laser was repetitively pulsed to accumulate the signal from a number of laser shots. The accumulated digital data for each channel at every 15–m–altitude bin along with the sum of the squares of the digital data for each bin are stored on magnetic disk for later analysis. A summary of the Raman lidar system characteristics is given in Table 13.

Total rejection of Rayleigh/Mie scattering at the laser wavelength (355 nm) by the interference filters is necessary for proper operation. Table 14 provides transmission values at 355 nm for each of the components of both filters. The data of Table 14 indicate that the transmission of the water-vapor and nitrogen filters at 355–nm approaches values

Table 13. System characteristics.

Laser wavelength	355 nm
Pulse energy	100 mJ
Laser repetition rate	10 pps
Telescope diameter	1.5 m
Raman water-vapor channel	
center wavelength	407.6 nm
filter width	4.8 nm
peak transmission	20.9%
Raman nitrogen channel	
center wavelength	387.5 nm
filter width	3.8 nm
peak transmission	25.1%

Table 14. Spectral filter component transmission at 355 nm.

Component	Transmission
Raman Water-Vapor Channel (407.6 nm)	
3 mm BG 36	0.0003
1 mm GG 395	0.011
1 mm BG 38	0.7
Blocker (Ag)	0.000015
Bandpass	0.00002
Raman Nitrogen Channel (387.5 nm)	
3 mm BG 36	0.0003
1 mm GG 375	0.12
2 mm BG 38	0.5
Blocker (Ag)	0.00001
Bandpass	0.00003

less than 10^{-15} and 10^{-14} respectively. Rejection of 355-nm radiation by the filters was verified during a field measurement by operating the system during cloud-cover conditions. No cloud-backscatter return was observed in either channel, indicating total rejection of Rayleigh/Mie scattering. The experiment was conducted during the night of 29/30 April 1985 at the NASA Goddard Space Flight Center in Greenbelt, Maryland, near Washington, D.C. On the 29th, the Maryland region was under the influence of high pressure centered over the Great Lakes. During the day the center of high pressure slowly drifted to the southeast. By the early morning of the 30th, the high-pressure region extended from the lower Great Lakes through the Carolinas. Conditions throughout the experiment period were dry and clear with thin patchy cirrus visible late in the evening of the 29th.

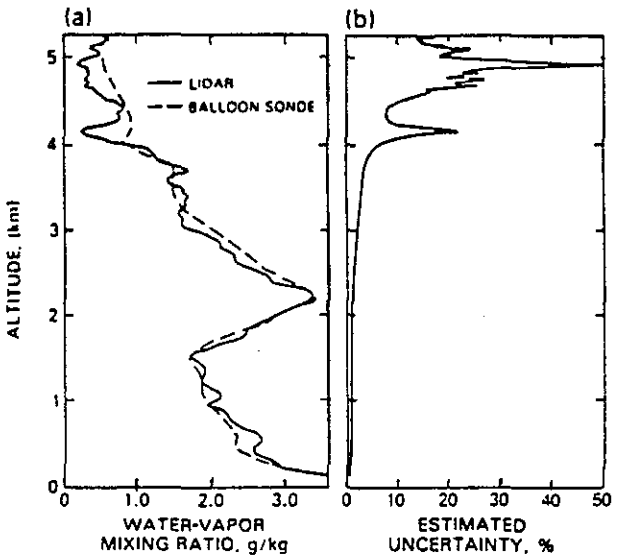

Figure 18. (a) Ratio of Raman scattering from water vapor to nitrogen compared with water-vapor mixing ratio from 0100–EDT radiosonde. (b) Calculated percent deviation of the lidar-derived water-vapor mixing ratio.

The good agreement between the lidar-derived mixing ratio and the balloon measurement as a function of altitude (Fig. 18a) along with the low (less than five percent) random uncertainty of the lidar data (cf. Fig. 18b) demonstrates that the lidar can be useful as a tool for observing atmospheric moisture.

More recently, Renaut and Capitini (1988) have shown that a Solar-Blind Raman lidar (SBRL) operating at 266 nm can measure humidity profiles with very good spatial resolution (30 m) during the day. The main disadvantage is its shorter range (1.2 km) which is due in part to the lower power and smaller telescope used and in part to O_3 absorption which must be accounted for by taking data on O_2, N_2, and H_2O Raman lines. The relative error in water vapor mixing ratio profiles measured with the SBLM aimed towards the zenith from the ground and from a drone flying at 3 km aimed towards the ground are shown in Fig. 19.

One option available is to use a combination of 355 and 266 nm Raman lidars the former for its better performance and range at night and the latter for its ability to operate during the day. Compared with the DIAL system the Raman approach requires a much less sophisticated laser but a much more powerful one and a high-quality optical receiver.

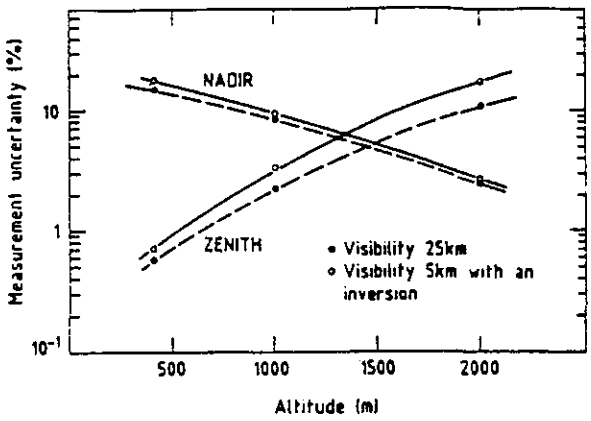

Figure 19. Relative error in the water-vapor mixing ratio profile measured from the ground (lidar aimed toward zenith) and from a drone flying at a height of 3000 m (lidar aimed toward nadir). Vertical resolution is 30 m and 1000 laser shots are averaged. Characteristics of the lidar are those of our SBRL. Two profiles of aerosols have been used for the computation: one with a ground visibility of 25 km and an exponential decrease, the other with a ground visibility of 5 km and an aerosol loaded layer up to 400 m. Other atmospheric parameters are as in 18a.

4.10 CO_2 Differential Absorption Lidar (DIAL)

Pulsed coherent CO_2 lidars have been employed to measure water vapor profiles by the differential absorption lidar (DIAL) technique (e.g., Hardesty, 1984).

Because the wavelength region between 9 and 11 μm is particularly rich with respect to absorption lines of various pollutants, such as ethylene, ammonia, ozone, perchloroethylene, trichloroethylene, and Freon 12, several groups have attempted DIAL measurements using incoherent CO_2 lidar systems. Although transmit pulse energies in some of these systems were >1 J, maximum ranges attainable using aerosol targets were typically in the 2–3-km range. Because of the exponential increase in total extinction with range, significantly extending the range capabilities of incoherent CO_2 DIAL systems probably necessitates substantial increases in laser pulse energy. Employment of coherent detection provides an alternative means of increasing the maximum range capability of such DIAL systems. The characteristics of the WPL Doppler lidar are given in Table 15.

Although these potential applications provide good reason to consider using coherent DIAL, the technique is not without its drawbacks. Coherent systems are typically more sensitive to speckle and refractive-index turbulence effects than direct detection systems are; hence, the advantage in mean SNR does not fully translate into improved measurement capability. Also, because coherent systems are more complex, their advantages have to be fairly significant to justify the added operational effort they require.

Table 15. WPL lidar system parameters.

Transmitter	
Pulse energy	100 mJ
Pulse duration	Nominal 2 μs
Pulse repetition frequency	10 Hz
Frequency control	Hybrid-TE configuration; closed loop servo control
Telescope	
Type	Off-axis paraboloid
Primary diameter	28 cm
Focal length	202 cm
Receiver	
Detector	HgCdTe photodiode
Local oscillator	Discharge-excited CO_2 laser
Bandwidth	10 MHz
Intermediate frequency	20 MHz
Computer-controlled scanner	
2-axis	
Pointing accuracy	0.1°

In the experiment described here, the NOAA lidar system was used to measure water vapor along both horizontal and slant paths. Because the lidar has been designed primarily for measuring winds, certain system characteristics such as transmit pulse duration and wavelength-switching techniques were suboptimal for the DIAL measurements. Despite this, water profiles were obtained to ranges of 10 km along horizontal paths and 6 km along slant paths. To the best of our knowledge, these are the first range-resolved coherent DIAL measurements. Previous coherent measurements have been reported which used ground-based or airborne CW systems or a ground-based pulsed lidar. Each of these systems, however, utilized returns from topographical or retroreflective targets.

The DIAL measurements were performed in the vicinity of Boulder, Colo., through the winter and spring of 1983. Typically, the winter atmosphere along the Front Range of the Rocky Mountains is extremely dry; mean absolute humidities range from ~2 g/m^3 at the surface to 0.4 g/m^3 at 500-mbar pressure (~4 km above ground level). Because of such low water vapor concentrations aloft, measurements during winter months were performed with the lidar directed horizontally so as to maximize the water vapor encountered by the beam. Horizontal measurements also permit the use of ground-based sensors to obtain necessary temperature measurements (for absorption cross-section adjustment) and water vapor comparison data.

The two water vapor concentration estimates made on 23 March are shown in Fig. 20, along with the mean of the estimates and an in situ temporally averaged water vapor concentration measurement taken simultaneously at the Boulder Atmospheric Observatory (~25 km away). The two profiles agree reasonably well with the point measure-

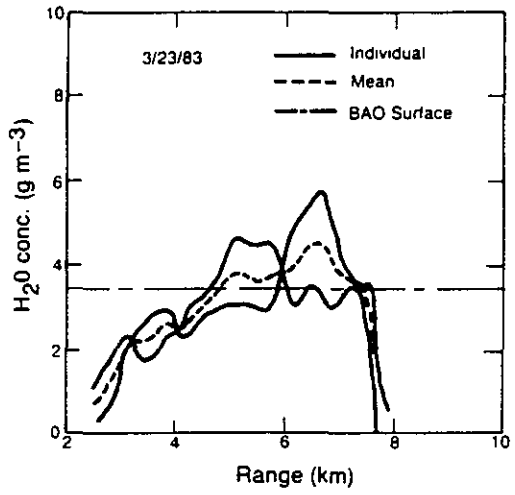

Figure 20. Water vapor concentration estimates vs. range for 23 March measurements. Long-dashed line shows mean concentration measured at ground station ~25 km away.

ment and with each other. Both DIAL profiles show a slight increase in concentration with range. Although there are no data available for comparison to indicate whether this is real or the result of some measurement artifact, the concentration might reasonably be expected to increase toward the west as the beam comes closer to the higher-elevation surface.

These results demonstrate the potential of coherent CO_2 DIAL for range-resolved species concentration measurements at longer ranges. Using a suboptimal system, we simultaneously measured water vapor concentrations and radial wind velocities to horizontal ranges beyond 10 km and to vertical heights approaching 5.5-km ASL. The measurements, obtained using a transmit-pulse energy of 100 mJ, illustrate the sensitivity advantage of heterodyne detection in the λ = 10.6-μm portion of the spectrum. Similar DIAL experiments employing direct detection resulted in maximum ranges of 2–3 km despite the use of order of magnitude more powerful laser transmitters. At shorter ranges ($\leq$2 km) direct detection is probably preferable to heterodyne detection for DIAL measurements, since the systems are less complex and less susceptible to speckle and turbulence effects.

Grant et al. (1987) have described CO_2 DIAL water vapor measurements using, in addition to the strongly absorbing 10.247 μm line, other CO_2 laser lines for which the absorption coefficients are weaker. They report agreement from 1–23%, the worst agreement being primarily for those lines where ammonia also absorbs strongly and for the weaker continuum absorption.

Technological improvements aiming towards higher pulse rates and more sturdy hardware are in progress. The solid state lidar is a potential candidate for this application. However, research is needed to

(1) establish the absorption parameters of the atmospheric constituents more precisely, and

(2) confirm accuracy of backscatter measurements when large numbers of pulses are averaged during coherent detection.

5. COMBINED SYSTEMS

The performance characteristics of proven and new remote sensing systems described in Chapters 3 and 4 make it abundantly clear that no single system, at least in present form, can meet the range and accuracy requirements for RAPS. Systems have to be used in combination to bridge gaps in their ranges or deficiencies in their performance. Attempts so far to measure winds and temperatures with combined systems have all been short term efforts associated with specific experiments or performance tests. However, with careful choice of systems and their operating parameters, there could be savings in hardware cost and reduction in the size of the integrated systems. The characteristics of the various systems described in this report are summarized in Fig. 21.

For a full-range Profiler system capable of measuring winds from 100 m to 17 km, one could use a 50 MHz/915 MHz Profiler combination such as the one tested by Ecklund et al. (1989) at Christmas Island (Fig. 22). The hybrid system yields profiles with good agreement where they meet (1.7–2 km). However, this is not a portable system and its best application would be in a base station providing fallout predictions and supporting the RAPS units. With RASS on the two profilers, temperature profiles up to 6 km can be routinely measured. The same wind coverage can be obtained with a 404 MHz/915 MHz hybrid, the only disadvantage being the shorter reach of the 404 MHz RASS ($\sim$3 km). This disadvantage is offset if the RASS information is combined with satellite retrievals to extend the temperature profile upward. The 3–5 km gap produces only a slight degradation in profiling accuracy.

For a transportable system capable of the 3 km range required for RAPS, we have several options. The portable 404 MHz Profiler with a smaller antenna but with more power than the one developed by WPL, and with RASS capability up to 3 km augmented at the low end with AL's proven 915 MHz Profiler/RASS system, the proposed Acoustically Enhanced Profiler (AEP) or even the 2 kHz Doppler sodar should prove adequate. The lower limit of the range can be extended down to 10 m with the 50 kH Doppler minisodar proposed in Chapter 4. A transportable 404 MHz IDI system would also provide winds up to 3 km with a smaller antenna but more complicated processing.

Pulsed Doppler lidars such as the WPL system described in Chapter 3, operating in a VAD mode and used in combination with the standard three beam 2 kHz Doppler sodar can also provide dependable vertical wind profiles from 50 m to well above 3 km. However, the lidar system as configured now is too bulky and too complex optically to even merit consideration as a component of RAPS. The high pulse rate CO_2 lidar under development could potentially overcome these limitations to provide winds to about the same height. The more compact systems such as the solid state and the wave guide lidars proposed in Chapter 4 offer promise of portability, better spatial resolution, and turn-key operation. Both these systems can achieve ranges up to 3–5 km, but the latter because of its lower power may encounter lower signal-to-noise ratios in returns above the atmosphere's boundary layer (1–2 km) when the aerosol concentrations above that layer drop significantly. The lidar systems have the advantage of being undetectable and less

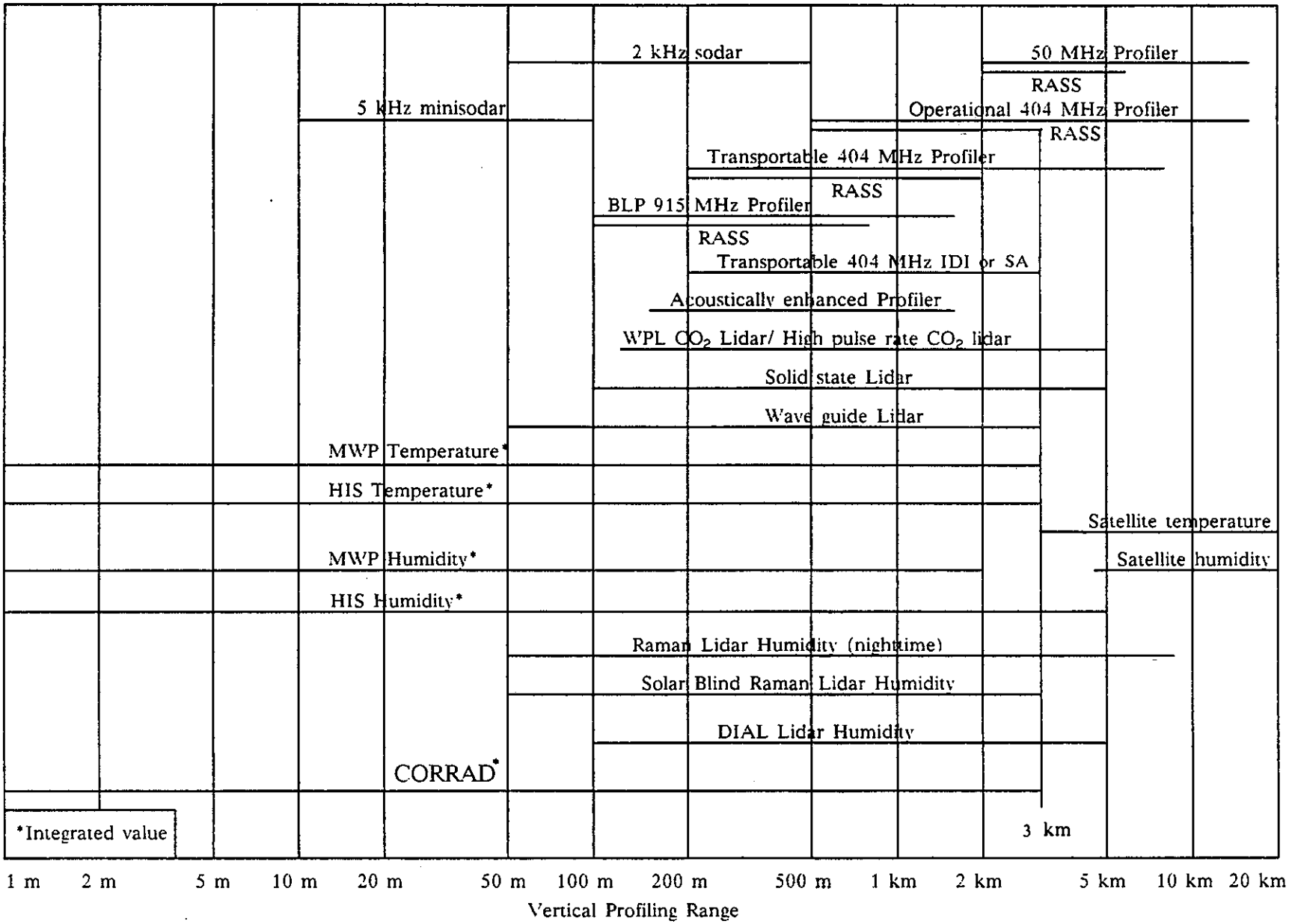

Figure 21 Vertical profiling range of remote sensing techniques.

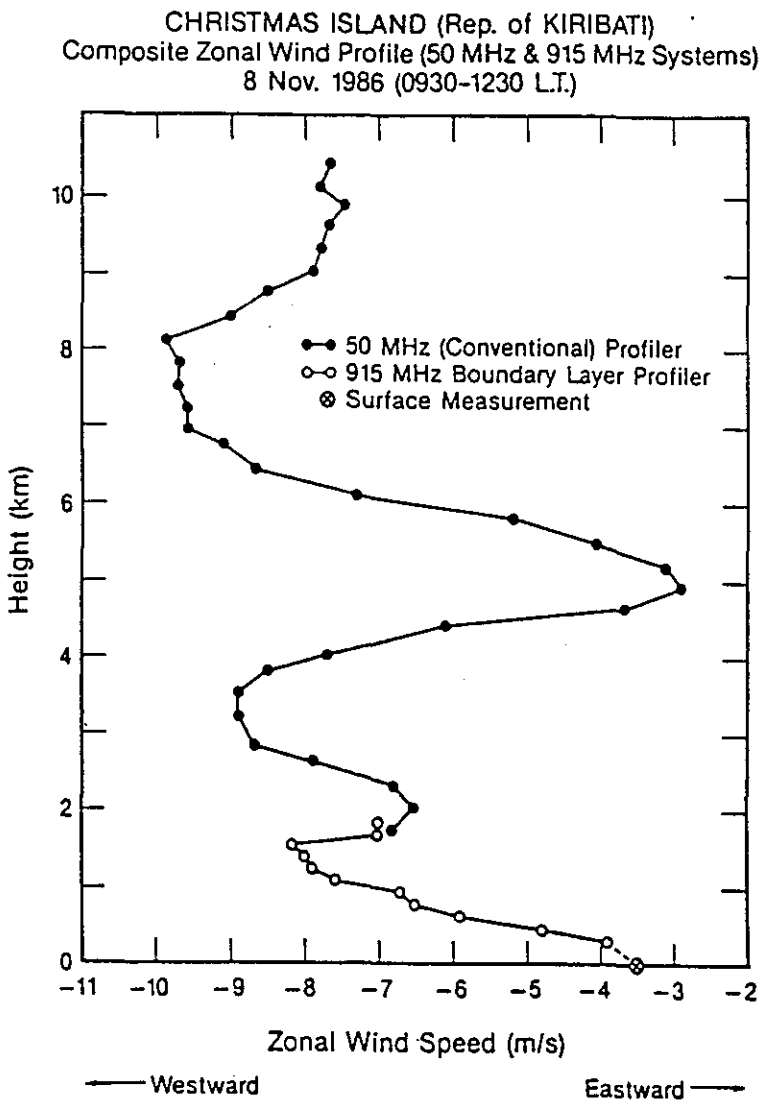

Figure 22. Composite zonal wind profile at Christmas Island.

obtrusive than the radar systems in the battlefield environment and can provide area coverage if needed up to 20 km with low angle scans, but their range is very much dependent on the existence of aerosols and the absence of fog, rain, snow and thick clouds. For this reason the lidar, in its more portable form, may serve as an auxiliary system to be activated under favorable conditions or when wider area coverage is desired. It should be pointed out that a lidar/sodar system will not provide temperature profiles and the choice for temperature coverage include MWP/satellite combination (for "quietness"), 915 MHz Profiler with RASS, the acoustically enhanced RASS or a combination of any of these systems.

A few comments on combining temperature profiling techniques are in order. Since the ground-based passive retrieval system (MWP) reliability above 5 km complements the increased satellite retrieval accuracy above 5 km, the two systems in combination provide

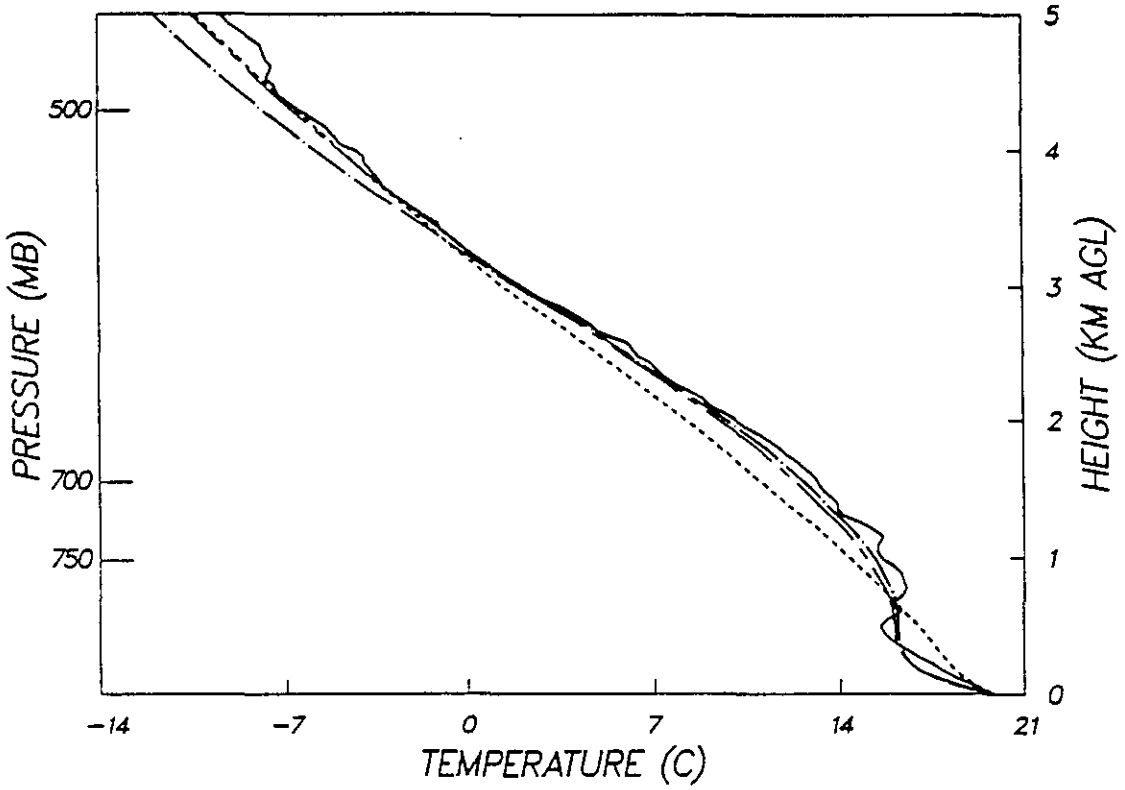

Figure 23. Comparison of soundings at 1700 UTC 3 August 1988; 16 RASS measurement levels; CLASS temperature sounding (——) with temperature soundings retrieved from MWP (---), RASS (- · -), and combined (——) systems.

temperature profiles of higher accuracy than either one can provide separately (Westwater et al., 1984). However, comparisons from soundings retrieved from MWP, 915 MHz RASS and CLASS (balloon) temperature soundings (Shroeder, 1989) has established that the RASS and the RASS/MWP combined retrievals more closely approximated the CLASS profile (Fig. 23) and that the difference between the two are not significant enough statistically to warrant the use of RASS and MWP in combination. (This is because the height range where the MWP weighting factors are the strongest is also the range where the RASS is the most accurate.) Cost considerations favor the RASS system in situations where a wind profiling radar is already in place. Thus the emerging consensus in WPL is that a 915 (or 404) MHz RASS/satellite combination represents an optimum configuration of temperature profiling in the troposphere.

Replacing MWP with HIS would provide no increased benefit (even though there might be distinct advantages in terms of vertical resolution and accuracy) because HIS covers the same height range as MWP and, more significantly, works only in fair weather and below cloud base. HIS/RASS combinations have yet to be investigated.

In selecting the satellite product for combining with RASS we have two options: the geostationary VAS, which have coverage only over the continental United States, or the polar orbiting TOVS which passes overhead twice a day. For application anywhere in the

world, TOVS would be the logical choice, but the temperature profile available for a given site may be as old as 12 h near the equator. At higher latitudes this delay is shortened because of the overlap in the TOVS footprints. In practice, however, the tactical units will have access to more current information from the polar orbiting DMSP (Defense Military Satellite Program) and from geostationary satellites operated by other countries. Their characteristics are superior in some respects to TOVS and VAS.

For humidity profiling, the options are more limited than for wind and temperature. A ground-based system consisting of the dual channel radiometer in MWP combined with HIS should provide the best coverage possible with current technology. The MWP is an all-weather device which also provides an accurate estimate of the total precipitable water up to 300 mb, but its output is the integrated value over the whole depth (the profile being deduced from a knowledge of surface moisture and climatology). HIS on the other hand operates only under clear conditions, but utilizes more water vapor lines to provide stronger signals and better vertical resolution. To insure reliability in the measurements, the MWP/HIS system should be operated in combination with RASS measuring temperature, since the temperature information is needed to establish the proper humidity profile and to establish the saturation humidity at cloud base in the presence of clouds. (The CORRAD system in its present form is not considered a strong enough candidate to be competitive with either MWP or HIS because of its smaller line strength.) In principle, as with temperature, the ground based measurements from the MWP/HIS system can be combined with satellite (geostationary or polar orbiting) for improved range and accuracy, but the benefits of combination have yet to be proven. The lidar techniques for measuring humidity are still years away from being ready for integration into an operational system with other remote sensors.

6. RECOMMENDED OPTIONS

Although a list of remote sensing options have been discussed in the previous chapters, narrowing down those options for application in RAPS requires careful weighing of range capability, cost and the risk involved. Table 16 provides a summary of all these factors. It should be emphasized that the ranges for virtually all systems vary by almost a factor of two, depending on atmospheric conditions.

The accuracies listed are nominal. They too can vary depending on atmospheric conditions. By increasing the averaging times, greater accuracies can be achieved, but the single most critical factor, is the presence of scatterers in the atmosphere. Whether it be velocity inhomogeneities, temperature inhomogeneities or aerosols, if the scatterers are not present, the remote sensors will indicate missing data or simply very low readings.

In Table 17 nine different options are presented to illustrate the types of combinations possible. They range from low-cost low-risk to high-cost high-risk. The low-cost options require some sacrifice in range whereas for higher costs and higher risks lidar systems for wind and humidity sensing becomes a possibility. Each combination is designed to be self-contained for measuring winds, temperatures, humidities and pressures. The low risk options can be implemented today with perhaps a modest development cost to optimize the 404-MHz antenna design. The higher risk options require more extensive development work and are several years away in terms of prototype design for mobile use.

Thus high risk should be viewed as a combination of technological feasibility and time to conduct development. Individual items with 30% or more risk will take a minimum of 3 to 5 years of development before they can be considered operational.

In developing criteria for high, medium and low costs, we defined combined systems costing less than $600K as low, $600K to $900K as medium and above $900K as high. Analogous criteria for risk factors are 25% or less for low, 25% to 65% for medium and above 65% for high.

Table 16. Summary of Profiling System Characteristics

Profiling System	Variable	Accuracy	Range (km)	Resolution Ht (m)	Resolution Time (min)	Cost ($)	Risk (%)	Comments
50-MHz Wind Profiler	Wind	1 ms^{-1}	2-15	50-600	6	350K	0	Not transportable
Operational Profiler	Wind	1 ms^{-1}	0.5-15	375,1000	6	400K	0	Not transportable
Transportable be 404-MHz Profiler	Wind	1 ms^{-2}	0.2-6	150,300	3	150K	0	Antenna could smaller
Transportable 404-MHz IDI	Wind	1.5 ms^{-1}	0.2-3	150,300	6	250K	50	Needs prototype development
Transportable 404-MHz SA	Wind	1.5 ms^{-1}	0.2-3	150,300	6	120K	30	Needs prototype development
915-MHz Boundary Layer Profiler	Wind	0.5 ms^{-1}	0.1-1.5	100,300	1	80K	0	Range could be increased with more power
Acoustically Enhanced Profiler	Wind, Temp	0.5 ms^{-1} 0.5°C	0.15-1.5	100,300	1	120K	5	Not fully tested
2-kHz Doppler Sodar	Wind	1 ms^{-1}	0.05-0.5	30	6	50K	0	Antennas could be smaller
5-kHz Doppler Minisodar	Wind	0.5 ms^{-1}	0.01-0.1	10	1	40K	0	Fully feasible

Table 16. Summary (continued)

Profiling System	Variable	Accuracy	Range (km)	Resolution Ht (m)	Resolution Time (min)	Cost ($)	Risk (%)	Comments
High pulse rate lidar	Wind	0.5 ms^{-1}	0.12-5	25-200	2	500K	20	Under development
10.6-μm WPL CO_2 Lidar	Wind	0.5 ms^{-1}	0.12-5	25-200	2	1M	0	Too bulky and optically
Solid State Doppler Lidar	Wind	0.1 ms^{-1}	0.1-5	5-50350	1	350K		Needs prototype development
Waveguide lidar	Wind	0.5 ms^{-1}	0.05-3	10-100	2	200K	30	Needs prototype development
MWP temperature Profiler	Temp	2°C	0-3	***	2 2	400K	0	Details of profile smoothed out
Above with satellite retrieval	Temp	2°C	0->15	***		550K*	0	Same as above but more accurate above 3 km
50-MHz RASS	Temp	1°C	2-6	150-600	6	50K**		Large acoustic source needed
404-MHz Operational RASS	Temp	1°C	0.5-3	375,1000	6	50K**	10	Not field tested
404-MHz transportable RASS	Temp	1°C	0.1-2	150,300	3	50K**	0	Field tested
915 MHz BLP RASS	Temp	1°C	0.1-1	100,300	1	30K**	0	Field tested

Table 16. Summary (continued)

Profiling System	Variable	Accuracy	Range (km)	Resolution Ht (m)	Resolution Time (min)	Cost ($)	Risk (%)	Comments
HIS	Temp, Hum	2°C 15%	0-5	***	2	100K	50	Operates only in clear weather below cloud base
CORRAD	Hum	20%	0-3	***	2	100K	75	Spectral lines weak affected by rain
Raman lidar (nighttime)	Hum	10%	0.05-3	25	6	175K	10	Most successful system operates only at night
Solar blind Raman lidar	Hum	10%	0.05-7	25	6	200K	20	Solar blind system, less reliable
DIAL Lidar	Hum	10%	0.1-5	200	2	300K	50	Experimental results relativity crude
MWP two channel humidity Profiler	Hum, total liquid water	20% 10%	0-2	***	2	100K	0	Affected by rain
Above with satellite retrieval	Hum	15%	0->15	***	2	200K	25	Same as above, not tested yet

* $100K included for satellite dish
** Above cost of Profiler
*** Integrated value adjusted according to climatology

Table 17. Cost-Risk Considerations for Available Options

HIGH COST, LOW RISK	HIGH COST, MED RISK	HIGH COST, HIGH RISK
o 404-MHz wind profiler with RASS o 2-kHz Doppler sodar o RASS/MWP/Satellite temperature retrieval o MWP/Satellite humidity retrieval	o Waveguide Doppler lidar o 915-MHz wind profiler with RASS o 5-kHz Doppler sodar o RASS/MWP/Satellite temperature retrieval o MWP/Satellite humidity retrieval	o Solid-state Doppler lidar o 915-MHz Acoustically Enhanced Profiler (AEP) o 5-kHz Doppler sodar o AEP MWP/Satellite temperature retrieval o Raman or DIAL lidar/ satellite humidity retrieval
MED COST, LOW RISK	**MED COST, MED RISK**	**MED COST, HIGH RISK**
o 404-MHz wind profiler with RASS o 2-kHz Doppler sodar o RASS/Satellite temperature retrieval o MWP/Satellite humidity retrieval	o Waveguide Doppler lidar o 915-MHz Acoustically Enhanced Profiler (AEP) o 2-kHz Doppler sodar o AEP/Satellite temperature retrieval o MWP/Satellite humidity retrieval	o 404-MHz IDI profile o 2-kHz Doppler sodar o HIS/Satellite temperature retrieval o HIS/Satellite humidity retrieval
LOW COST, LOW RISK	**LOW COST, MED RISK**	**LOW COST, HIGH RISK**
o 915-MHz wind profiler with RASS o 5-kHz Doppler sodar o RASS/Satellite temperature retrieval o MWP/Satellite humidity retrieval	o 915-MHz Acoustically Enhanced Profiler (AEP) o 5-kHz Doppler sodar o AEP/Satellite temperature retrieval o MWP/Satellite humidity retrieval	o 404-MHz SA profiler o 2-kHz Doppler sodar with 915-MHz RASS o RASS/Satellite temperature retrieved o MWP/Satellite humidity retrieval

7. REFERENCES

Adams, G.W., D.P. Edwards, and J.W. Brosnahan, 1985: The imaging Doppler interferometer: data analysis. Radio Sci., 20, 1481–1492.

Briggs, B.H., B. Candy, W.G. Elford, W.K. Hocking, P.T. May, and R.A. Vincent, 1984: The Adelaide VHF radar–capabilities and future plans. URSI/SCOSTEP Workshop on Technical Aspects of MST Radar, Urbana, Illinois, May 22–25, 1984. Handbook for MAP, 14, University of Illinois, Urbana, 357–359.

Briggs, B.H., G.I. Phillips, and D.H. Shinn, 1950: The analysis of observations on spaced receivers of the fading of radio signals. Proc. Phys. Soc., 63B, 106–121.

Chadwick, R.B., 1988: The Wind Profiler Demonstration Network. Preprints, Lower Tropospheric Profiling Symposium, Boulder, Colorado, May 31–June 3, 1988. American Meteorological Society, Boston, 109–110.

Clifford, S.F., T. Wang, and J.T. Priestley, 1978: Spot size of the radar returns from a Radar Acoustic Sounding System (RASS) due to atmospheric refractive turbulence. Radio Sci., 13, 985–989.

Clough, S.A., R.D. Worsham, W.L. Smith, H.E. Rivercomb, R.O. Knuteson, H.W. Woolf, G.P. Anderson, M.L. Hoke, and F.X. Kneizys, 1988: Validation of FASCODE Calculations with HIS Spectral Radiance Measurements. International Radiance Symposium, Lille, France.

Ecklund, W.L., D.A. Carter, and B.B. Balsley, 1988: A UHF wind profiler for the boundary layer: Brief description and initial results. J. Atmos. Oceanic Technol., 5, 432–441.

Ecklund, W.L., K.P. Moran, P.E. Currier, B.L. Weber, D.A. Carter, and D.B. Wuertz, 1988: A Comparison of 915, 405 and 50 MHz Wind Profiling Radars. Preprints, Lower Tropospheric Profiling Symposium, Boulder, Colorado, May 31–June 3, 1988. American Meteorological Society, Boston, 123–124.

Ecklund, W.L., D.A. Carter, B.B. Balsley, K.S. Gage, and P.E. Currier, 1989: Recent developments in lower tropospheric wind profiling. Proc., First European Wind Profiler Workshop, Versailles, France, March 6–8, 1989, C33–C44.

Gage, K.S., and B.B. Balsley, 1978: Doppler radar probing of the clear atmosphere. Bull Amer. Meteor. Soc., 59, 1074–1093.

Gage, K.S., and J.L. Green, 1979: Tropopause detection of partial specular reflection with very–high–frequency radar. Science, 203, 1238–1240.

Grant, W.B., J.S. Margolis, A.M. Brothers, and D.A. Tratt, 1987: CO_2 DIAL measurements of water vapor. Appl. Opt., 26, 3033–3041.

Hall, F.F., Jr., R.M. Huffaker, R.M. Hardesty, M.E. Jackson, T.R. Lawrence, M.J. Post, R.A. Richter, and B.F. Weber, 1984: Wind measurement accuracy of the NOAA pulsed infrared Doppler lidar. Appl. Opt., 23, 2503–2506.

Hardesty, R.M., 1984: Coherent DIAL measurement of range-resolved water vapor concentration. Appl. Opt., 23, 2545-2553.

Harris, C.M., 1966: Absorption of air versus humidity and temperature. J. Acoust. Soc. Amer., 40, 148-160.

Hogg, D.C., M.T. Decker, F.O. Guirard, K.B. Earnshaw, D.A. Merritt, K.P. Moran, W.B. Sweezy, R.G. Strauch, E.R. Westwater, and C.G. Little, 1983: An automatic profiler of wind, temperature and humidity. J. Clim. Appl. Meteor., 22, 807-831.

Kane, T.J., W.J. Kozlovsky, R.L. Byer, and C.E. Byvik, 1987: Coherent laser radar at 1.06 micrometer using Nd:YAG 1 lasers. Opt. Lett., 12, 239.

Kon, A.I., 1984: Combined effect of wind and turbulence on the signal intensity in Radio Acoustic Sounding of the atmosphere. Izves. Atmos. Oceanic Phys., 21, 942-947.

Krans, J.D., 1966: Radio Astronomy. McGraw Hill: New York, 254-555.

Lataitis, R.J., S.F. Clifford, and P.T. May, 1990: Tropospheric wind profiling using radar "interferometry," NOAA Tech. Mem. ... Wave Propagation Laboratory, NOAA/ERL, Boulder, Colorado (to be published).

Lawrence, T.R., B.F. Weber, M.J. Post, R.M. Hardesty, R.A. Richter, N.L. Abshire, and F.F. Hall, Jr., 1986: A comparison of Doppler lidar, rawinsonde, and 915-MHz UHF wind profiler measurements of tropospheric winds. NOAA Tech. Mem., ERL WPL-130, NOAA/ERL, Boulder, Colorado, 84 pp.

McAllister, L.G., 1968: Acoustic sounding of the lower troposphere. J. Atmos. Terr. Phys., 30, 1439-1440.

Melfi, S.H., and D. Whiteman, 1985: Observation of lower atmospheric moisture structure and its evolution using a Raman lidar. Bull. Amer. Meteor. Soc., 66, 1285-1292.

Masuda, Y., 1988: Influence of wind and temperature on the height limit of a radio-acoustic sounding system. Radio Sci., 23, 647- 654.

May, P.T., and R.G. Strauch, 1989: An examination of wind profile signal processing algorithms. J. Atmos. Oceanic Technol., 6, 731-735.

McMillin, L.M., and C. Dean, 1982: Evaluation of new operational technique for producing clear radiance. J. Appl. Meteor., 21, 1005-1014.

Miller, P.A., and M.J. Falls, 19889: The incorporation of inversion characteristics into cloud-based microwave temperature soundings: A Simulation Study, Microwave Remote Sensing of the Earth System, A. Chedin, Editor, A. Deepak Publishing, Hampton, Virginia, 51-73.

Moran, K.P., R.G. Strauch, K.B. Earnshaw, D.A. Merritt, B.L. Weber, and D.B. Wuertz. 1989: Preprints, 24th Conference on Radar Meteorology, Tallahassee, Florida, March 27–31, 1989, American Meteorological Society, Boston, 728–731.

Neff, W.D., and R.L. Coulter, 1986: Acoustic remote sensing, Probing the Atmospheric Boundary Layer, D.H. Lenschow, Editor. American Meteorological Society, Boston, Massachusetts, 201–239.

Peters, G., 1989: Temperature and wind profilers from radar wind profilers equipped with acoustic sources. Proc., First European Wind Profiler Workshop, Versailles, France, March 6–8, 1989, C85–C90.

Phillips, N.A., L.M. McMillin, D. Wark, and A. Gruber, 1979: An evaluation of early operational temperature sounding from TIROS–N. Bull. Amer. Meteor. Soc., 60, 1188–1197.

Rivercomb, H.E., H. Buij's, H.B. Howell, D.D. LaPorte, W.L. Smith, and L.A. Stromorsky, 1988: Radiometric calibration of IR Fourier transform spectrometers: Solution to a problem with the High resolution Interferometer Sounder (HIS). Appl. Optics, 27, 3210– 3218.

Rottger, J., and P. Czechowsky, 1980: Tropospheric and stratospheric wind measurements with the spaced antenna drifts technique and the Doppler beam swinging technique using a VHF radar. Preprints, 19th Conference on Radar Meteorology, Miami, Florida, April 15–18, 1980, American Meteorological Society, Boston, 577–584.

Rottger, J., and H.M. Ierkic, 1985: Postset beam steering and interferometer applications of VHF radars to study winds, waves, and turbulence in the lower and middle atmosphere. Radio Sci., 20, 1461–1480.

Ruf, C.S., 1987: Atmospheric profiling of water vapor and liquid water with a K–band autocorrelation radiometer. Ph.D. dissertation University of Massachusetts, 164 pp.

Ruf, C.S., and C.T. Swift, 1988: Atmospheric profiling of water vapor density with a 20.5–23.5 GHz autocorrelation radiometer. J. Atmos. Oceanic Technol., 5, 539–546.

Schroeder, J.A., 1989: A comparison of temperature soundings obtained from simultaneous radiometric, radio acoustic and rawinsonde measurements. J. Atmos. Oceanic Technol. (in press).

Smith, W.L., 1970: Iterative solution to a radiative transfer equation for the temperature and absorbing gas profile of an atmosphere. Appl. Optics, 9, 1993–1999.

Smith, W.L., V.E. Suomi, W.P. Menzel, H.M. Woolf, L.A. Sromovsky, H.E. Rivercomb, C.M. Hayden, D.N. Erickson, and F.R. Mosher, 1981: First sounding system results from VAS–D. Bull. Amer. Meteor. Soc., 62, 232–236.

Smith W.L., H.M. Woolf, D.Q. Wark, and L.M. McMillin, 1979: The TIROS-N operational vertical sounder. Bull. Meteor. Soc., 60, 1177-1187.

Smith, W.L., H.E. Rivercomb, H.B. Howell, and H.M. Woolf, 1983: HIS-A satellite instrument to observe temperature and moisture profiles with high vertical resolution. Preprints, Fifth Conference on Atmospheric Radiation, Baltimore, Maryland, October 31 - November 4, 1983, American Meteorological Society, Boston, 1-9.

Strauch, R.G., D.A. Merritt, K.P. Moran, K.B. Earnshaw, and D. van de Kamp, 1984: The Colorado wind profiling network. J. Atmos. Oceanic Tech., 1, 37-49.

Strauch, R.G., K.P. Moran, P.T. May, A.J. Bedard, and W.L. Ecklund, 1988: RASS temperature sounding techniques. NOAA Tech. Mem. ERL WPL-158. NOAA/ ERL, Boulder, Colorado, 12 pp.

Volek, M.J., 1989: Atmospheric wind measurements using a 50 MHz Imaging Doppler Interferometer. Master's Thesis, Utah State University, Logan, Utah, March 1989. CASS Report #GR-09.

Westwater, E.R., and O.N. Strand, 1968: Statistical information content of radiation measurement used in indirect sensing. J. Atmos. Sci., 25, 750-758.

Westwater, E.R., W.B. Sweezy, L.M. McMillin, and C. Dean, 1984: Determination of atmospheric temperature profiles from a statistical combination of ground-based profiler and operational NOAA 6/7 satellite retrievals. J. Clim. Appl. Meteor., 23, 689-703.

Westwater, E.R., W. Zhenhui, N. Grody, and L.M. McMillin, 1985: Remote sensing of temperature profiles of a combination of observations from the satellite-based microwave sounding unit and the ground-based profiler. J. Atmos. Oceanic Technol., 2, 97-109.

Woodman, R.F., 1971: Inclination of geomagnetic field measured by an incoherent-scatter technique. J. Geophys. Res., 76, 178-184.